Seismic chimney characterisation in the North Sea – Implications for pockmark formation and shallow gas migration.

Ben Callow[1,2*], Jonathan M. Bull[1], Giuseppe Provenzano[1,3], Christoph Böttner[4], Hamza Birinci[1], Adam H. Robinson[1], Timothy J. Henstock[1], Timothy A. Minshull[1], Gaye Bayrakci[5], Anna Lichtschlag[5], Ben Roche[1], Naima Yilo[1], Romina Gehrmann[1], Jens Karstens[4], Ismael H. Falcon-Suarez[5], Christian Berndt[4].

[1]University of Southampton, School of Ocean and Earth Science, Southampton, SO14 3ZH, UK.

[2]Ghent University, Department of Geology, PProGRess/UGCT, Ghent, Belgium.

[3]University of Grenoble Alpes, ISTerre, Grenoble, France.

[4]GEOMAR Helmholtz-Centre for Ocean Research Kiel, Kiel, Germany.

[5]National Oceanography Centre, Waterfront Campus, Southampton, SO14 3ZH, UK.

Corresponding author: Ben Callow, E-mail: ben.callow@ugent.be

Abstract

Fluid-escape structures within sedimentary basins permit pressure-driven focused fluid flow through inter-connected faults, fractures and sediment. Seismically-imaged chimneys are recognised as fluid migration pathways which cross-cut overburden stratigraphy, hydraulically connecting deeper strata with the seafloor. However, the geological processes in the sedimentary overburden which control the mechanisms of genesis and temporal evolution require improved understanding. We integrate high-resolution 2D and 3D seismic reflection data with sediment core data to characterise a natural, active site of seafloor methane venting in the UK North Sea and Witch Ground Basin, the Scanner pockmark complex. A regional assessment of shallow gas distribution presents direct evidence of active and palaeo-fluid migration pathways which terminate at the seabed pockmarks. We show that these pockmarks are fed from a methane gas reservoir located at 70 metres below the seafloor. We find that the shallow reservoir is a glacial outwash fan, that is laterally sealed by glacial tunnel valleys. Overpressure generation leading to chimney and pockmark genesis is directly controlled by the shallow geological and glaciogenic setting. Once formed, pockmarks act as drainage cells for the underlying gas accumulations. Fluid flow occurs through gas chimneys, comprised of a sub-vertical gas-filled fracture zone. Our findings provide an improved understanding of focused fluid flow and pockmark formation within the sediment overburden, which can be applied to subsurface geohazard assessment and geological storage of CO_2.

Keywords: Chimneys, Pipes, Overburden, Pockmarks, Fluid flow, North Sea, CO_2 sequestration, Glacial stratigraphy.

1 Introduction

Greenhouse gases, such as methane (CH_4) and carbon dioxide (CO_2) may be naturally or artificially sequestered within porous and permeable subsurface reservoirs (Bachu, 2000; Benson and Cole, 2008; Ringrose and Meckel, 2019; Global CCS Institute, 2020). Subsurface reservoirs are commonly overlain by impermeable cap rocks and low-permeability overburden stratigraphy, that prevent the upward migration of fluids to the seabed (Furre et al., 2017). However, seal bypass, or fluid-escape systems are geological features that may permit cross-stratal, pressure-driven fluid migration from deeper strata to the seabed (Cartwright et al., 2007; Løseth et al., 2009; Andresen, 2012). Fluid-escape from the subsurface may include anthropogenic sources, such as abandoned wells (e.g., Watson & Bachu, 2009; Böttner et al., 2020), and natural sources, such as migration up-dip along permeable stratigraphic horizons (e.g., Tóth, 1980; Hindle, 1997; Lloyd et al., 2021), and the formation or reactivation of fluid escape structures (e.g., Nichols et al., 1994; Frey et al., 2009; Cartwright et al., 2021). The type of fluid flow which occurs can be dependent on subsurface lithological and stress conditions. Therefore, constraining the physical properties of fluid pathways and the mechanisms of fluid flow is critical for the risk assessment of potential subsurface fluid escape. Where fluid-escape pathways extend to the seabed, understanding the rate of gas release from offshore seeps is required to quantify more accurately the input of greenhouse gases into the atmosphere and hydrosphere (Ligtenberg & Connolly, 2003; Leifer & Boles, 2005; Greinert et al., 2010; Shakhova et al., 2010). Annual global methane emissions sourced from natural geological sources are estimated as 18-63 Mt, with offshore seeps contributing 5-10 Mt and considerable uncertainty in the estimates (Etiope et al., 2019a; Etiope et al., 2019b; Saunois et al., 2020).

Seismic reflection imaging can identify focused fluid-escape conduits. One class of these features are seismic chimneys (e.g., Hustoft et al., 2010) or pipes (e.g., Moss & Cartwright, 2010a), collectively referred to herein as chimneys. Chimneys are vertical to sub-vertical anomalies with circular or elliptical planforms observed in seismic reflection data (e.g., Løseth et al., 2011; Robinson et al., 2021). Within seismic chimney structures, seismic amplitude blanking and discontinuous/chaotic reflections are generally observed (e.g., Løseth et al., 2011; Robinson et al., 2021). Chimneys have been observed

extensively from seismic imaging, both throughout the North Sea (Hovland & Sommerville, 1985; Cole et al., 2000; Bünz et al., 2003; Karstens & Berndt, 2015), and globally (e.g., Cartwright et al., 2007; Gay et al., 2007; Moss & Cartwright, 2010a,b; Løseth et al., 2011; Plaza-Faverola et al., 2017). If fluid were to migrate from a sub-surface reservoir of CO_2/CH_4 and reach the base of these chimneys, then they could act as a pathway for fluids, allowing upward migration towards the seafloor, and ultimately into the water column (Robinson et al., 2021). However, the geological processes which control the genesis and spatial distribution of focused fluid conduit formation, and the vertical fluid transmissivity of these pathways (i.e. permeability), require further constraint.

Chimney formation on a small scale has been observed during a number of controlled subseafloor gas release experiments, including the QICS and STEMM-CCS experiments (Taylor et al., 2015; Cevatoglu et al., 2015; Flohr et al., 2021; Roche et al., 2021). Time-lapse seismic reflection data acquired prior to, during, and after the completion of gas release, were used to observe the development of a chimney over time. The results of these experiments indicate that these chimney structures form during upward propagation of the gas through two principal processes - fracture generation, and reactivation of pre-existing fractures in fine-grained sediment (Cevatoglu et al., 2015; Roche et al., 2021). In shallow (low effective stress), fine-grained, poorly consolidated sediments, conditions for new fracture generation are favourable, which may be a primary process for chimney formation at shallow depths (Fauria & Rempel, 2011). Upward propagation of fluids may also occur through capillary flow processes, which is the favoured mechanism under higher effective stress conditions (Cathles et al., 2010). Additional process mechanisms proposed for chimney initiation include erosive fluidisation, syn-sedimentary formation and local subsurface volume reduction (Lowe, 1975; Sun et al., 2013; Cartwright & Santamarina, 2015).

Large-scale (~100-1000 m wide) chimneys are hypothesised to be comprised of a network of interconnected fractures oriented sub-vertically or radially. This permits the upward flow of gas in the sedimentary overburden (Bull et al., 2018), due to the resulting elevated permeability relative to matrix permeability of the host strata sediment (Cartwright et al., 2007; Marin-Moreno et al., 2019). In this study, we test this hypothesis using direct observations to gain an improved understanding of large-

scale focused fluid conduit genesis, through the assessment of an active fluid-escape system in the Central North Sea, the Scanner pockmark complex.

The Scanner pockmark complex was chosen as an ideal site to characterise focused fluid conduits as it is the location of vigorous and persistent methane venting (Hovland and Sommerville, 1985; Judd and Hovland, 2009; Gafeira and Long, 2015; Li et al., 2020). Pockmarks are seabed depressions, created by the release of over-pressured pore-water and/or gas emission from the subsurface (Hovland et al., 2010; Cathles et al., 2010). The Scanner pockmark complex overlies the East Mey Storage Site, an area assessed for subsurface CO_2 storage potential (ACT Acorn Consortium, 2018; Alcalde et al., 2019). Li et al. (2020) used broadband acoustic measurements from the water column to determine the gas flux from Scanner as between 1.6 and 2.7 x 10^6 kg/year (272 – 456 L/min at the seafloor conditions). Sub-surface imaging also indicates the presence of bright spots at shallow depth, and chimney structures have been imaged on seismic reflection data to depths of several hundred metres (Bull et al., 2018; Böttner et al., 2019).

We used a variety of seismic sources (which include chirp and sparker) to collect high-quality seismic reflection images at Scanner. We interpreted these images together with industry 3D reflection data and analysis of sediment cores to constrain the physical characteristics of focused fluid conduits and determine the primary process mechanisms of fluid flow. The multi-frequency seismic data acquisition allowed high fidelity imaging of the sub-surface, including a better distinction between seismic artefacts and real geological structure, which is a major novelty of this study with respect to many previous chimney characterisation studies (e.g. Karstens & Berndt, 2015; Karstens et al., 2019a). Our direct observations permit the interpretation of focused fluid conduit genesis and temporal evolution. This paper has three main objectives:

1) We aim to understand the role and significance of the regional geological setting in the formation of chimneys and pockmarks, which is achieved through detailed characterisation of the stratigraphy and structural features at the Scanner pockmark complex.
2) We aim to gain additional insight into the depth and primary sources of gas governing the formation of chimneys and pockmarks. We address this aim by determining the spatial distribution of

subsurface gas accumulation to devise an interpretation of active and palaeo fluid migration pathways.

3) Finally, we aim to synthesise our findings into a schematic model of pockmark genesis and chimney formation, and discuss how our findings can be used to improve our understanding of focused fluid conduit and pockmark formation within the shallow overburden, for applications to subsurface geohazard assessment and CO_2 storage.

2 Geological Background

2.1 Scanner pockmark complex

The Scanner pockmark complex is situated in licence block UK 15/25 of the North Sea, close to the centre of the Witch Ground Basin (Fig. 1a). At this site, chimneys are observed directly below natural active seabed methane ebullition sites (Fig. 2), which include the Alkor, Challenger, Scanner and Scotia pockmarks (Gafeira and Long, 2015). The Alkor, Scanner and Scotia pockmarks are all compound pockmark features, each comprising two adjacent individual pockmarks (Fig. 2a). At the Scanner pockmark Complex, the large pockmarks (class 1 of Böttner et al., 2019), East and West Scanner are each >75 m wide, >250 m long and >15 m deep. West Scanner pockmark (Fig. 2c) emits methane (CH_4) into the water column episodically at a flux rate of 1600-2600 kg/day (Li et al., 2020), composed of a mixed biogenic and thermogenic source (Clayton & Dando, 1996). CH_4 venting is additionally evidenced by the presence of methane derived authigenic carbonates (MDACs) at the seabed (Judd et al., 1994; Judd & Hovland, 2009). Smaller pockmarks (class 2 of Böttner et al., 2019) are also distributed ubiquitously across the area (>1500 across 225 km^2; Fig. 2a) oriented NNE/SSW, in alignment with the tidal flow direction (Gafeira et al., 2012). Class 2 pockmark genesis is ascribed to localised pressure changes and sediment dewatering (Böttner et al., 2019).

2.2 Regional tectonics & stratigraphy

The study area is located within the Witch Ground Graben, which forms part of a Jurassic NW/SE trending horst-graben system (Fig. 1; Boldy & Brealey 1990). The present day stress field is tectonically controlled within the Witch Ground Graben, and the minimum horizontal stress direction ($\sigma 3$) is ~54°

(Evans & Brereton, 1990; Zanella & Coward, 2003). The Witch Ground Graben was a depocentre for Late Jurassic to Late Cretaceous sediments, including the Kimmeridge Clay Formation (Ahmadi et al. 2003). The Early to Late Cretaceous stratigraphic units pinch out towards the east, which may provide a zone of enhanced pore fluid pressure at the Witch Ground basin margins/Fladen Ground Spur (Fig. 1b; Copestake et al. 2003). The stratigraphic units of the Quaternary, Nordland Group and Hordaland Group prograde towards the east and south (Copestake et al. 2003). Therefore, regional-scale, buoyancy-driven fluid migration may be expected to occur towards the north and west, up-dip towards the basin margins (Fig.1b; Tóth, 1980).

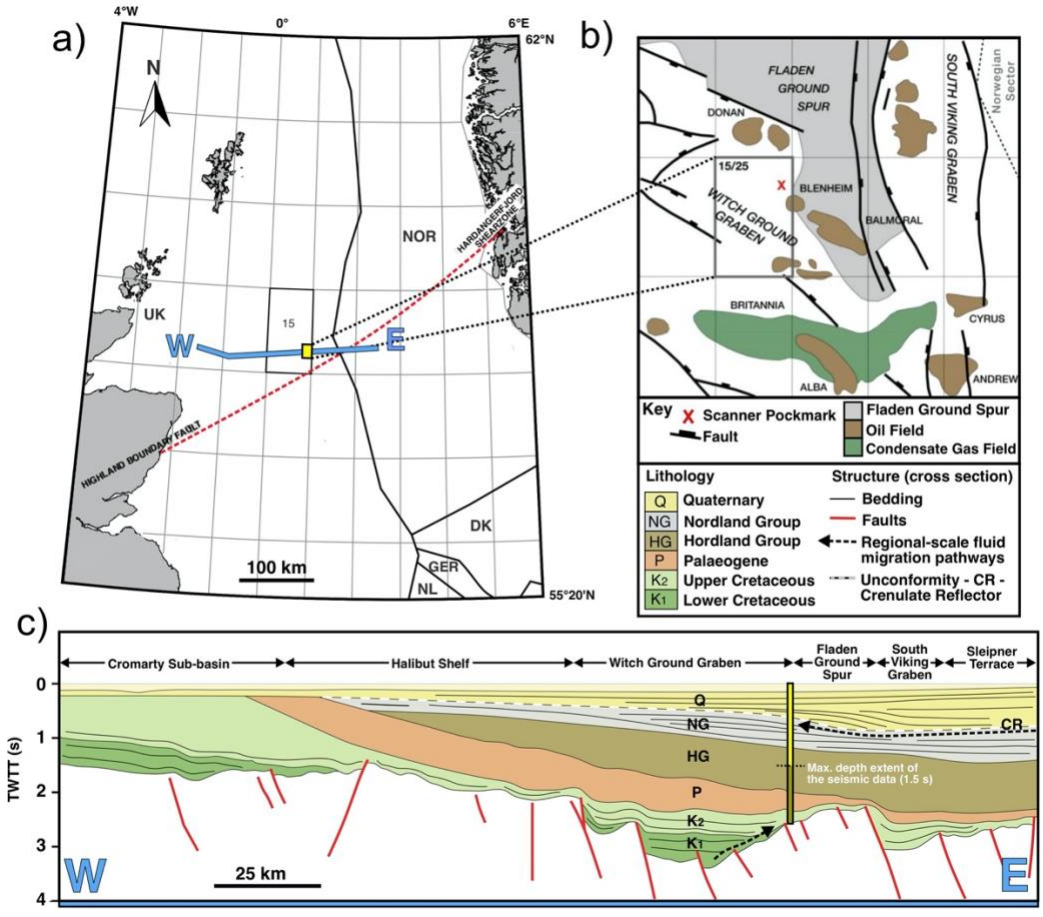

Fig. 1. Regional geological and structural setting of the Witch Ground Basin in the North Sea. **(a)** Map and position of regional seismic line (blue line) shown in (c). The study area (yellow box, licence block 15/25) is highlighted. **(b)** Structural map of the Witch Ground Graben. In the area of interest, the horst-graben basement structure is orientated NW/SE. **(c)** A regional geological cross section, trending west to east across the Central North Sea and the Witch Ground Graben, after Copestake et al. (2003). Six stratigraphic zones are highlighted. The study area is indicated by the vertical yellow line. Dashed arrows indicate regional-scale fluid migration pathways.

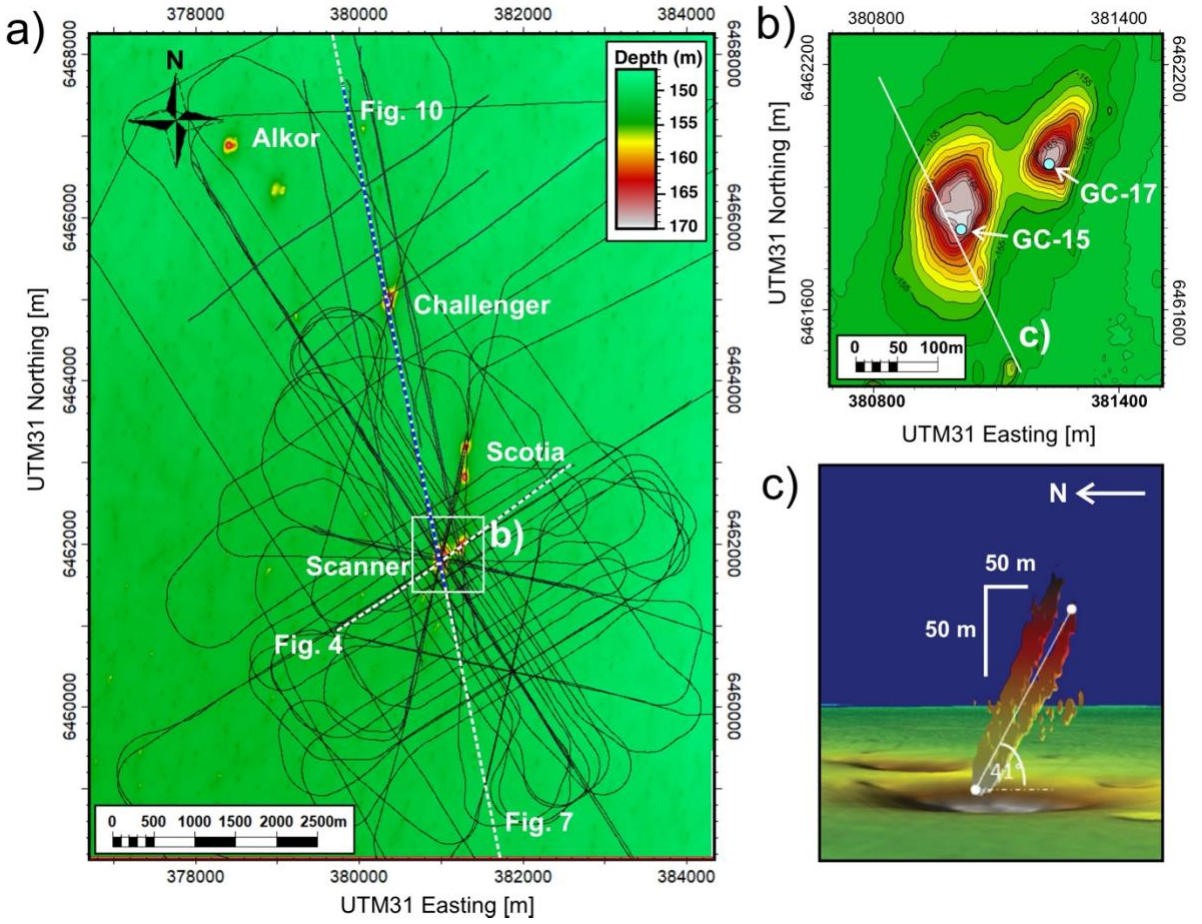

Figure 2. Bathymetry map of the Scanner pockmark complex together with the position of Sparker seismic reflection profiles collected during JC152. (a) Bathymetry map highlights the four large pockmarks: Scanner, Scotia, Challenger and Alkor, within a 75 km^2 area. Black lines show position of Sparker seismic reflection profiles. Dashed white and blue lines show locations of seismic data profiles shown in Figs. 4, 7 and 10. White box indicates area shown in b). **(b)** Seabed bathymetry, displaying East and West Scanner with GC-15 and GC-17 showing locations of the sediment core analysed. **(c)** Forked methane plume at West Scanner imaged by an EM710 multibeam echo sounder (70-100 kHz), after Li et al. (2020).

2.2.1 Stratigraphy and seismostratigraphic framework

Figure 3 provides a summary of the lithostratigraphy and seismostratigraphic framework of the Scanner pockmark complex study area. The ~300 m-thick Quaternary sediment succession deposited within the Witch Ground Basin was previously described by Stoker et al. (2011), Böttner et al. (2019) and Robinson et al. (2021). The Quaternary succession is underlain by the Nordland and Hordaland Groups, of Neogene and Palaeogene age respectively, that are composed of claystone with limestone and sandstone interbeds (Fig. 3; Judd et al.,1994). The top of the Nordland Group marks a regional

unconformity with the overlying Quaternary sediments, defined as the Crenulate Reflector, CR (Fig. 3). The base Quaternary unit, the Aberdeen Ground Formation (Fm.; unit S1 in Figs. 3-4), is composed of layered sands, silts and clay-rich sediments deposited in the Early Pleistocene (up to Marine Isotope Stage, MIS, 13), and displays a layered seismic character (Stoker et al., 2011; Ottesen et al., 2014). The Ling Bank Fm. (S2) erodes into the top of the underlying Aberdeen Ground Fm. (S1), representing a regional glacial unconformity, with sediment deposition occurring in the Early to Middle Pleistocene (MIS 12 to 10; Stewart & Lonergan, 2011; Reinardy et al., 2017; Böttner et al. 2019). Unit S2 is comprised of two subunits (Fig. 3), which are analogous to the sub-facies in glacial tunnel valley systems in the North Sea (e.g. Kluiving et al. 2003; Graham et al. 2007). The basal unit (S2.1) represents the lower unit of tunnel valley sediment infill, composed of coarse sands and gravels. Unit 2.1 displays a chaotic seismic character, that becomes more layered at shallower depths (Figs. 3-4). Unit S2.2 is composed of clay-rich sediment displaying no apparent seismic heterogeneities (ii) and coarse sands characterised by higher amplitude reflections (iii)(Figs. 3-4).

The Coal Pit Fm. (S3) overlies the Ling Bank Fm., and comprises Upper-Mid to Late Pleistocene (MIS 6-3) aged glacial tills (muddy sands; Andrews et al., 1990; Stoker et al., 2011). Units S2.2 (ii) and S3 have similar seismic facies separated in sparker data by a discontinuous reflector and are therefore indistinguishable in some areas (Figs. 3-4). The Coal Pit Fm. (S3) is conformably overlain by Last Glacial Maximum (LGM) deposits (S4), which comprises silty-sandy clays with rare pebbles, deposited during MIS 3 to 2 (Fig. 3). Units S3-S4 extend upwards to the base of Scanner pockmark. Units S3-S4 display a dim and chaotic seismic character, and are conformably overlain by the Witch Ground Fm. (S5). Unit S5 is composed of silty clay and is deposited during MIS 2 to 1 (Stoker et al., 2011). The Witch Ground Fm. has two main units: the lower (S5.1) and upper (S5.2) Witch Ground Members, respectively. Unit S5.2 has an interbedded seismic character, while unit S5.1 displays a uniform seismic character (Stoker et al., 2011), though the seismic boundary between these does not represent a significant change in sediment geotechnical properties (Paul & Jobson, 1991). The Scanner pockmark depression erodes down to the base of unit S5. High amplitude zones interpreted as gas-saturated sediment layers are observed at three discrete horizons, that include: 1) the Crenulate Reflector (CR),

2) the top of unit S2.2 (iii) and 3) the base of unit S5 (Fig. 4), as previously described by Böttner et al. (2019) and Bayrakci et al. (2021).

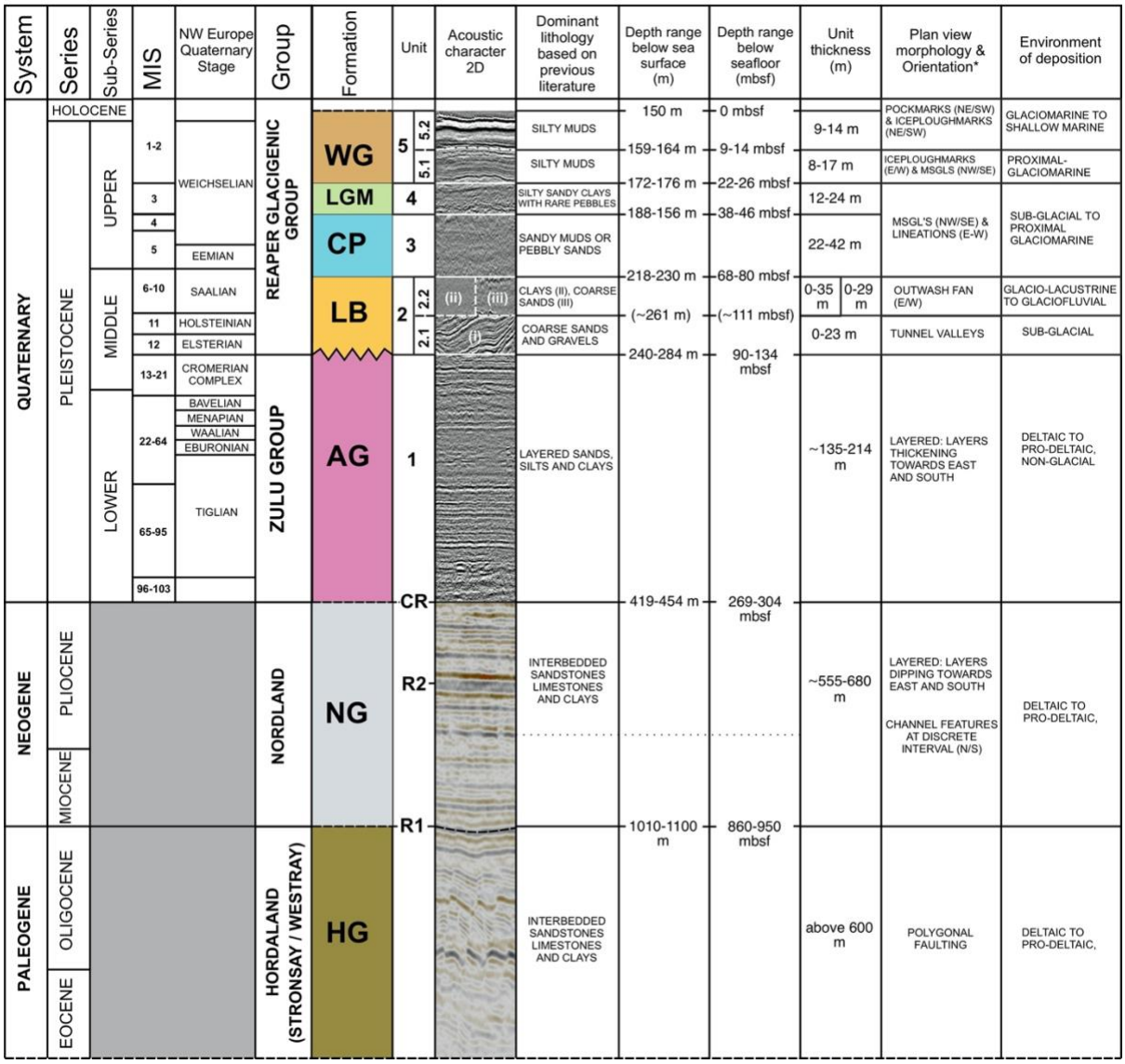

Figure 3. Summary of the Scanner pockmark complex chronostratigraphy, seismostratigraphy and lithostratigraphy. WG - Witch Ground, LGM - Last Glacial Maximum Deposits, CP - Coal Pit, LB - Ling Bank, AG - Aberdeen Ground, NG - Nordland Group and HG - Hordaland Group (also know as Stronsay or Westray Group). CR - Crenulate Reflector, which marks the Pliocene to Pleistocene boundary. The summary has been created from a synthesis of Robinson et al. (2021), Böttner et al. (2019), Ottesen et al. (2014), Stewart & Lonergan (2011), Stoker et al. (2011), Judd et al. (1994) and Andrews et al. (1990). The interpreted lithological sub-units of S2 (i, ii and iii) are derived from the previous classifications of Graham et al. (2007) and Kluiving (2003). The acoustic character column displays higher frequency surface sparker above CR and lower frequency 3D seismic data below CR.

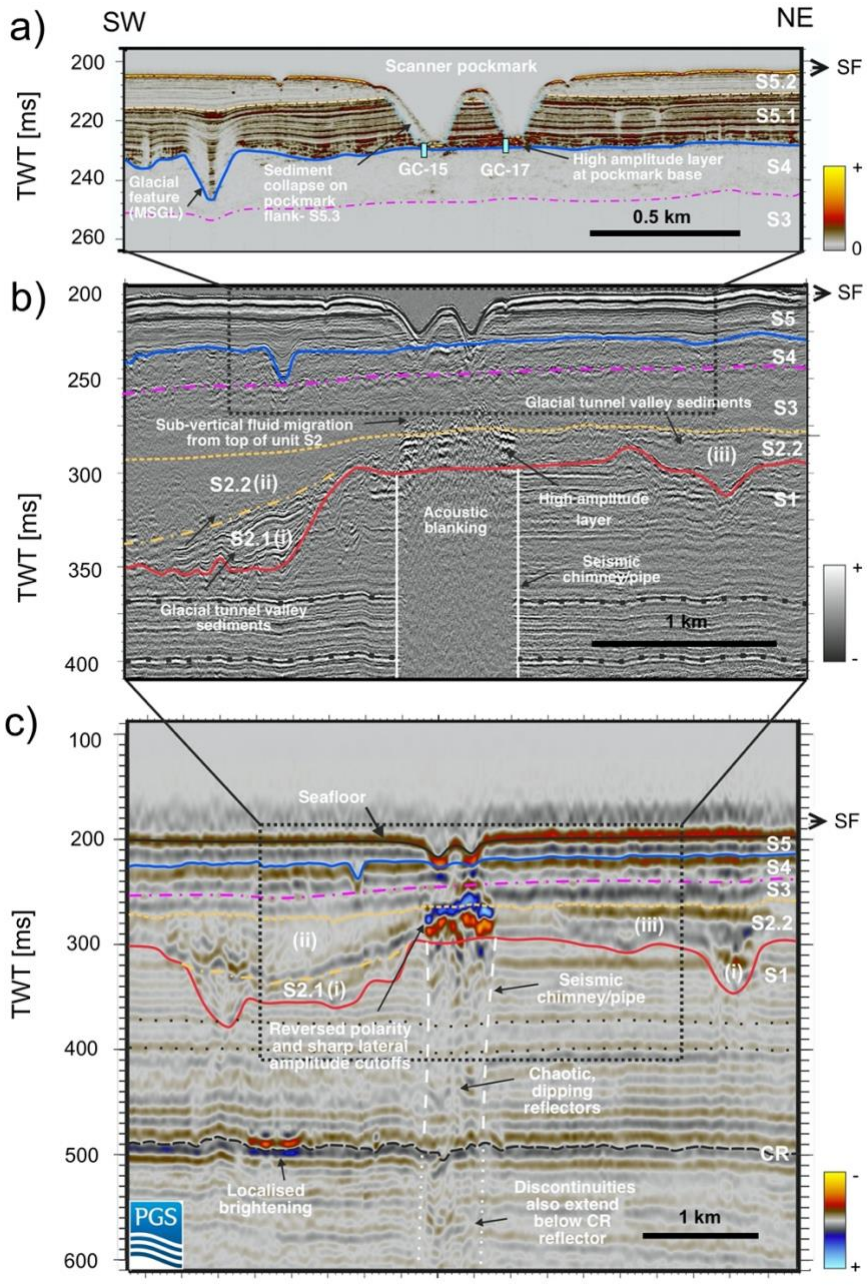

Figure 4. Seismostratigraphy of the Scanner pockmark region imaged using three different seismic sources along the same profile (location in Fig. 2a). (a) Sub-bottom profiler seismic reflection data. **(b)** Squid 2000 sparker seismic reflection profile. **(c)** Profile from airgun 3D seismic reflection data. CR - Crenulate Reflector (top of Nordland Group), S1 – Aberdeen Ground Fm., S2 – Ling Bank Fm., S3-4 – Coal Pit Fm. (S3 – Coal Pit & S4 – Last Glacial Maximum deposits (LGM)), S5 – Witch Ground Fm. (S5.1 – Fladen Member, S5.2 – Witch Member, S5.3 - Glen Member). Black dashed line = CR; red line = top S1; orange dot-dashed line = top S2.1; orange dashed line = top S2.2; pink dot-dashed line = top S3; blue line = top S4; pale brown dashed line = top S5.1 and black line = top S5.2 / SF = Seafloor. Outline of a chimney is displayed with a sub-vertical white dashed line. Location and depth extent of gravity cores GC-15 and GC-17 are displayed in (a). Figure after Robinson et al. (2021).

3 Data & methods

3.1 Seismic reflection data acquisition and processing

2D seismic reflection data were acquired using two different types of acoustic sources (Chirp sub-bottom profiler and surface sparker) to achieve a depth of penetration between 20 and 300 m below seabed (Bull, 2017). The multi-frequency seismic data acquisition allows high fidelity imaging of the sub-surface, including a better distinction between seismic artefacts and real geological structure. The Applied Acoustics Squid 2000 surface sparker source spans the frequency range between 100-1500 Hz; the source was fired at 1750-2000 Joules, with a 2 s interval, corresponding to a 4 m spacing, and recorded by multichannel streamers. Squid sparker profiles were acquired across the Scanner and Challenger pockmarks and processed using the time-domain workflow detailed in Provenzano et al. (2020). Each 2D post-stack time migrated section has a horizontal resolution of 2 m (common depth point, CDP, spacing) and a vertical tuning-thickness resolution of <0.45 m. In addition, single-channel SBP profiles were acquired using a 2.8-6 kHz bandwidth and 4.4 kHz central frequency. Each SBP profile has a horizontal and vertical spatial resolution of 2.5 m and <15 cm, respectively. These 2D high-frequency data were integrated with lower frequency 3D seismic data processed and provided by PGS (part of the CNS MegaSurveyPlus). The 3D data studied covers an area > 500 km^2 and depth of 1.5 s two-way travel time (TWTT), providing significant regional spatial coverage. Detailed analyses were performed on an area of 75 km^2 (Fig. 2). The full stack dataset has a 12.5 m CDP spacing and approximately 5-10 m vertical resolution. The 2D and 3D seismic reflection data was depth converted using a velocity model described in Robinson et al. (2020), that is comparable to the velocity model of Schramm et al. (2019). Seismic data are presented with the SEG European polarity convention, whereby an increase in impedance yields negative amplitude (soft reflection) displayed in red for the 3D seismic data and black for the sparker data.

3.2 Sediment sampling

Sediment cores were collected from beneath Scanner pockmark using a gravity corer during research cruise MSM78 (Karstens, 2019b). A maximum penetration depth of ~6 mbsf (meters below seafloor)

was achieved beneath the Scanner pockmark. X-ray micro-CT imaging of core sub-sections were collected, permitting the analysis of sediment structure and texture. Multi-Sensor Core Logging (MSCL) measurements of density were collected from split cores. In addition, grain size data was measured with a Malvern grain size analyser.

4 Results

4.1 Structural and glacial features

The multiple seismic reflection datasets were used to identify and map the structural features at the Scanner pockmark complex, in order to constrain potential focused fluid migration pathways. We describe our structural observations in stratigraphic order, beginning with the deepest identified features.

4.1.1 Polygonal faulting – Hordaland Gp.

Polygonal faulting is observed in the 3D seismic data volume at > 860 mbsf depth (950 ms TWTT), at the top of the Hordaland Gp. (Fig. 3) within the PGS 3D volume (Fig. 5). A total of 983 faults were measured across a 75 km^2 area. A length-weighted histogram reveals that the most common polygonal fault directions are 050-060° and 090-100° (Fig. 5). Typically, polygonal faults that form due to compaction and dewatering related phenomena show no preferential fault orientations (Cartwright et al., 2003). However, polygonal faults that form within a system of active tectonic stresses may show preferential fault orientations (Cartwright et al., 2003). The fault direction of 050-060° matches the regional minimum principal stress direction, suggesting that the orientation of the polygonal fault system is partly influenced by the regional tectonic stresses. The absence of direct hydrocarbon indicators within the polygonal faulted zone suggests that the polygonal fault system is not part of a shallow gas fluid migration system.

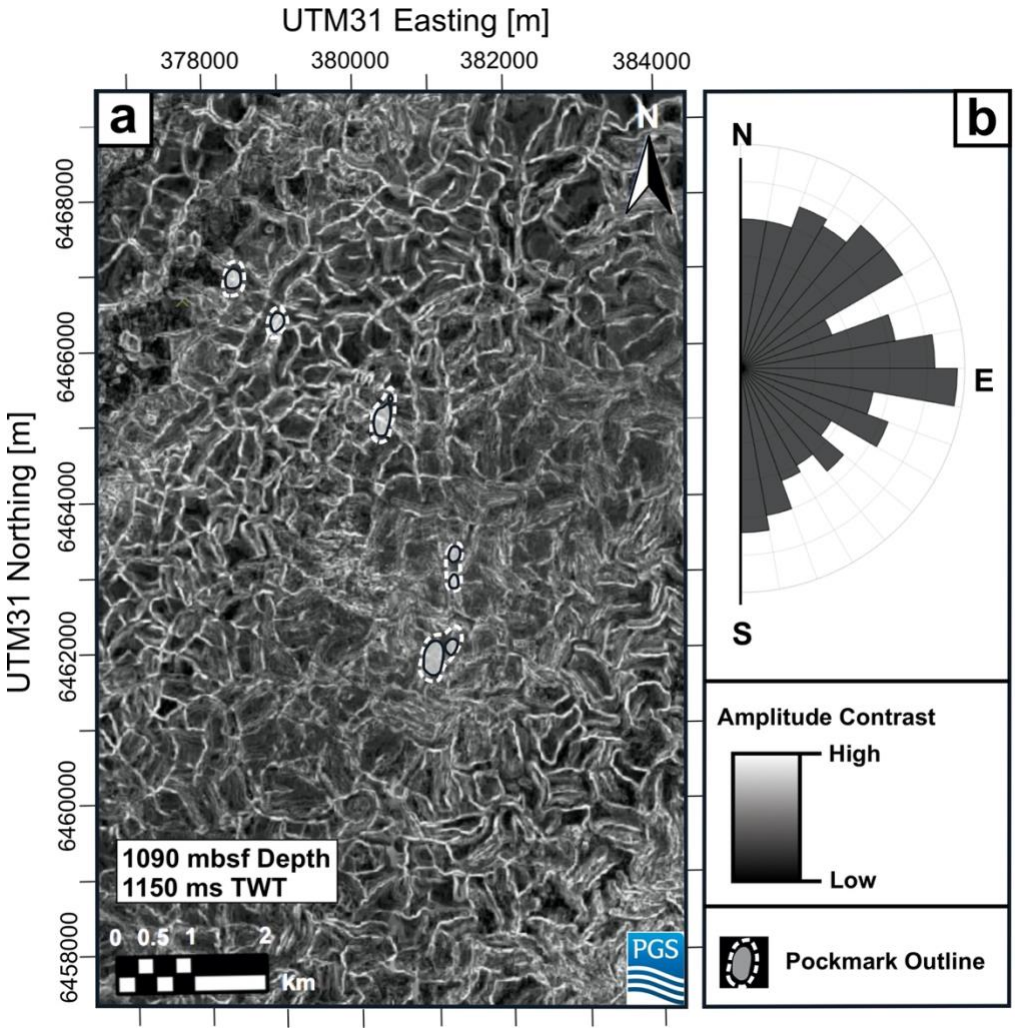

Figure 5. Mapping of the polygonal fault system, located at 1090 metres below seafloor (mbsf; Top Hordaland Group) from 3D seismic reflection data. (a) Surface attribute map of amplitude contrast at a constant depth of 1090 mbsf, with high amplitude contrast (white) highlighting the polygonal faults. Locations of the large pockmarks are displayed using a grey fill and white dotted outlines. **(b)** Fault orientation histogram (length-weighted histogram, 10° degree bins) showing preferential orientations at 050° and 090°. For clarity, figures 5, 6, 8 and 9 are depth maps (mbsf), with two-way-time (TWT) values only provided to allow comparison to the seismic profiles displayed in Figures 4, 7, 8 and 10-12.

4.1.2 Regional-scale features – Nordland Gp. and Aberdeen Ground Fm.

Surface maps of the Crenulate Reflector (CR) surface at ~270-305 mbsf depth (500 ms TWTT), have been generated from the 3D seismic volume to identify structural features (Fig. 6). Overall, this reflector dips toward the southeast (Fig. 6a). Seismic amplitude analysis of the CR surface reveals high amplitude lineations oriented at 070° and 160°. In cross section, these features display localised amplification of

negative amplitude with respect to the regional CR interface (Fig. 4). The localised high amplitude features have distinct v- and u-shaped cross-sections with lateral thicknesses of > 70 m (Fig. 4), when observed perpendicular to the lineations observed in map view (Fig 6b). A N-S seismic section provides an additional perspective of the CR, which displays a higher amplitude response compared to background reflectivity (Fig. 7). There are breaks in the seismic continuity of the CR surface beneath both the Scanner and Challenger pockmarks (Fig. 7a). These seismic discontinuities are oriented sub-vertically and extend upwards through unit S1 to high amplitude anomalies within unit S2.2 (Fig. 7a). Unit S2.2 hosts several seismic amplitude anomalies (Fig 7a) that are connected in planform view, and extend laterally along the entire margin of a glacial tunnel valley (Figure 8b; see section 4.2.1). In some areas, the base of the tunnel valley intersects the CR (Fig. 8a). The high amplitude anomalies of unit S2.2, with amplification by an order of magnitude with respect to background reflectivity, display reversed polarity and sharp lateral cut-offs in amplitude (Figs. 4,7). An independent controlled source electromagnetic (CSEM) study by Gehrmann et al. (2021) observed that the high amplitude anomalies also display a sharp resistivity increase with respect to background values.

We interpret that the amplitude anomalies within unit S2.2 are direct hydrocarbon indicators (DHIs), which represent a gas-saturated interval. The planform geometry of the interpreted gas-saturated zone indicates that gas is pooling along the margin of the tunnel valley (Fig. 8b; see section 4.2.1). Below Challenger pockmark, and adjacent to the tunnel valley, the interpretation of a gas-saturated layer located at 340 ms depth (Fig 7a), in addition to the discontinuities that intersect and overlie the CR suggest that there is a likely hydraulic connection between the CR and unit S2.2 (Fig. 8). We interpret that the discontinuities are most likely fractures, which can act as migration pathways. The alternative interpretation that the discontinuities between CR and S2.2 are attenuation artefacts could be assessed and validated by future seismic undershooting and reprocessing, travel time tomography and seismic anisotropy studies (Robinson et al. 2021). The localised amplitude brightening within the CR is most likely to be lithological, and the v-and u-shaped cross sections suggest they are sand-filled furrows, which can act as high permeability preferential pathways for regional-scale fluid flow. Overall, we infer a structurally-controlled, hydraulic connection between the CR and the overlying unit S2.2 (Fig. 7b).

Using the 3D seismic data, a large-scale discontinuity can be identified beneath a glacial tunnel valley (TV2) adjacent to Challenger pockmark (Fig. 7a). The maximum vertical depth extent of this seismic feature is not fully clear from the seismic reflection data, but appears to be ~900 ms TWTT (Fig. 7a). Seismic artefacts are commonly observed beneath tunnel valleys, and are referred to as type-C anomalies by Karstens & Berndt (2015). We infer that the seismic discontinuity is most likely an artefact, created by a combination of velocity pull-up beneath the tunnel valley caused by high density sediment infill of unit S2.1 and velocity pull-down from a gas-saturated horizon within unit S2.2 (Fig 7-8). Velocity pull-up and pull-down beneath areas of increased and reduced seismic velocities, caused by higher velocity tunnel valley sediment infill (Kluiving et al. 2003) and lower velocity pore-fluid, respectively, can cause apparent changes in the structural dips observed in time-domain (TWTT) seismic data, which has created the false appearance of a regional fault structure (Holmes & Stoker, 2005; Frahm et al., 2020). This would also explain why the seismic feature becomes less observable at increasing depth beneath the tunnel valley.

Additional seismic artefacts interpreted from the N-S reflection profile include surface-related multiples, peg-leg multiples and acoustic blanking (Fig. 7a; white circles). After discounting these artefacts, no DHIs are observed beneath the large pockmarks below the Crenulate reflector (CR).

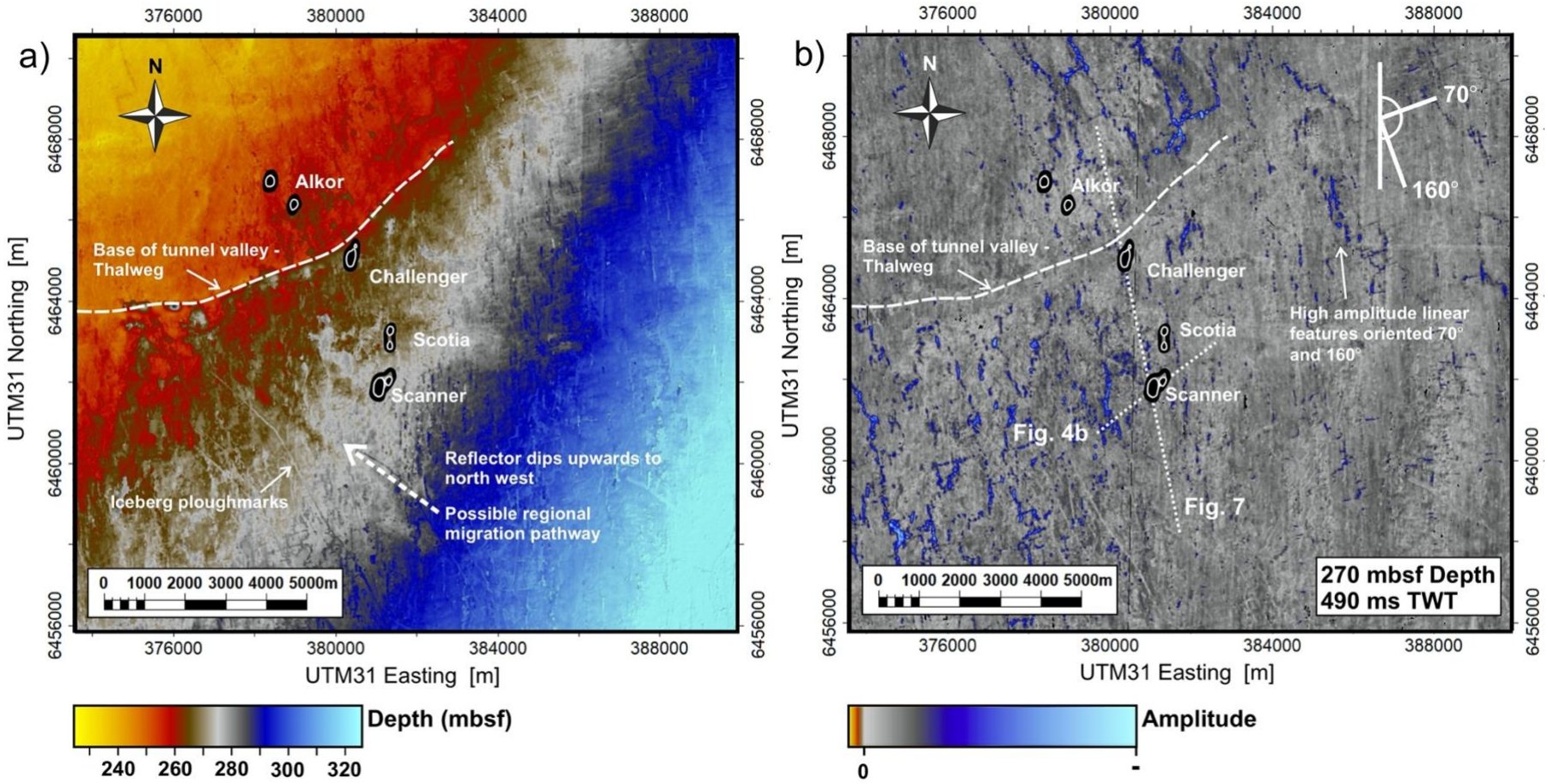

Figure 6. (a) Depth and (b) amplitude maps of Crenulate Reflector (CR) from 3D seismic reflection data. The reflector CR dips downwards to the south-east, which may permit regional-scale fluid migration northwards and westwards. **(b)** Displayed is a minimum amplitude map with a 10 ms window of extraction. High amplitude negative polarity lineations with v- and u-shaped cross sections are interpreted as sand-filled channels. The base of a tunnel valley intersects this horizon, which may provide a preferential zone for upward fluid-escape/drainage. Locations of the large pockmarks are displayed using a black fill and white outline. Dotted white line shows the location of seismic data profile shown in Fig. 7.

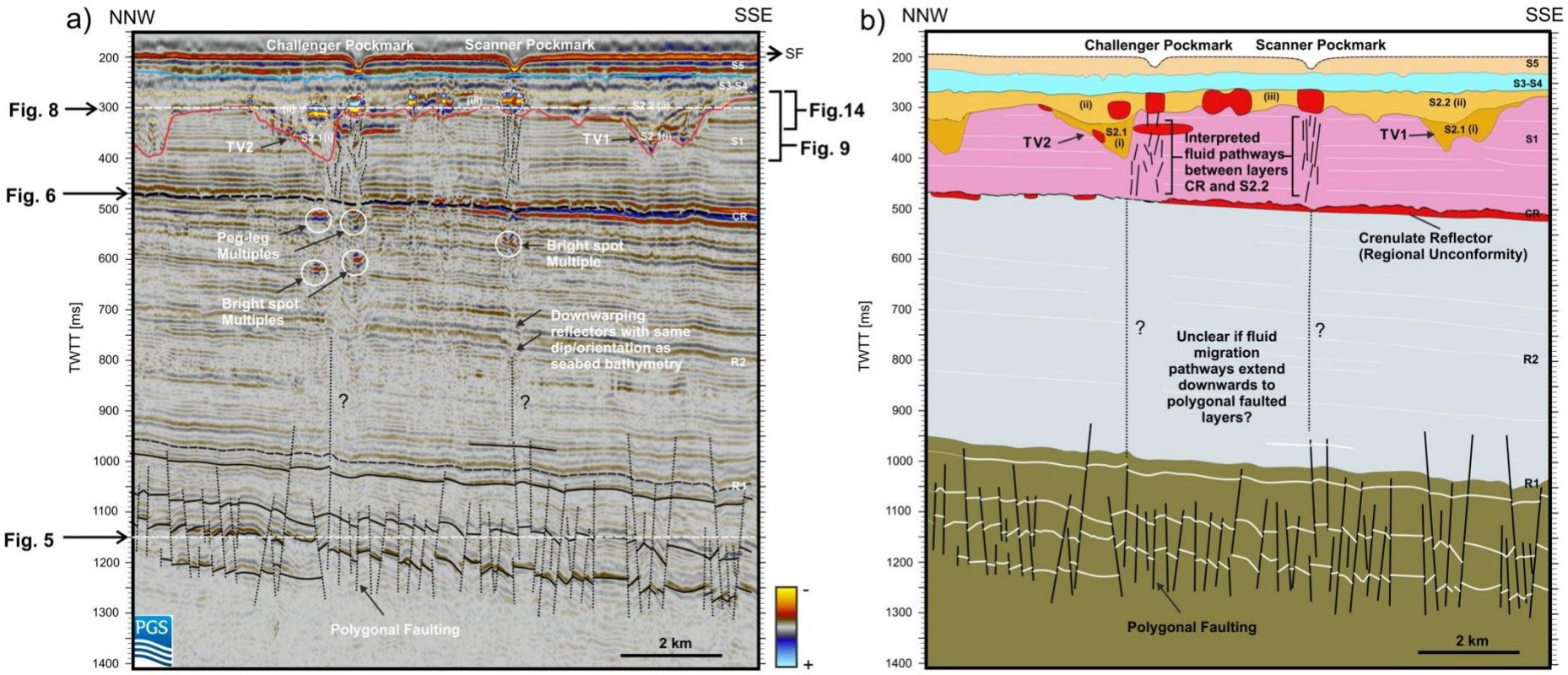

Figure 7. Seismic reflection section from the 3D volume and associated geological interpretation of the Scanner pockmark complex (position shown in Fig. 2). (a) Annotated seismic profile. **(b)** Geological interpretation, highlighting areas of gas accumulation at distinct stratigraphic intervals, including reflector unit S2.2. A hydraulic connection is interpreted between the horizons of reflector CR and unit S2.2. Seismic artefacts are interpreted below reflector CR. The presence and abundance of seismic artefacts caused by a combination of: 1) Seabed bathymetry/ pockmark geometry; 2) glacial tunnel valley geometry and; 3) bright spots within unit S2.2, prevents a conclusive interpretation of the presence of fluid pathways below reflector CR. The colour of the reflectors and units are the same as described in Figs. 3 and 4, respectively. White dashed circles – bright spots; White circles – interpreted bright spot and peg-leg multiples. TV – Tunnel Valley.

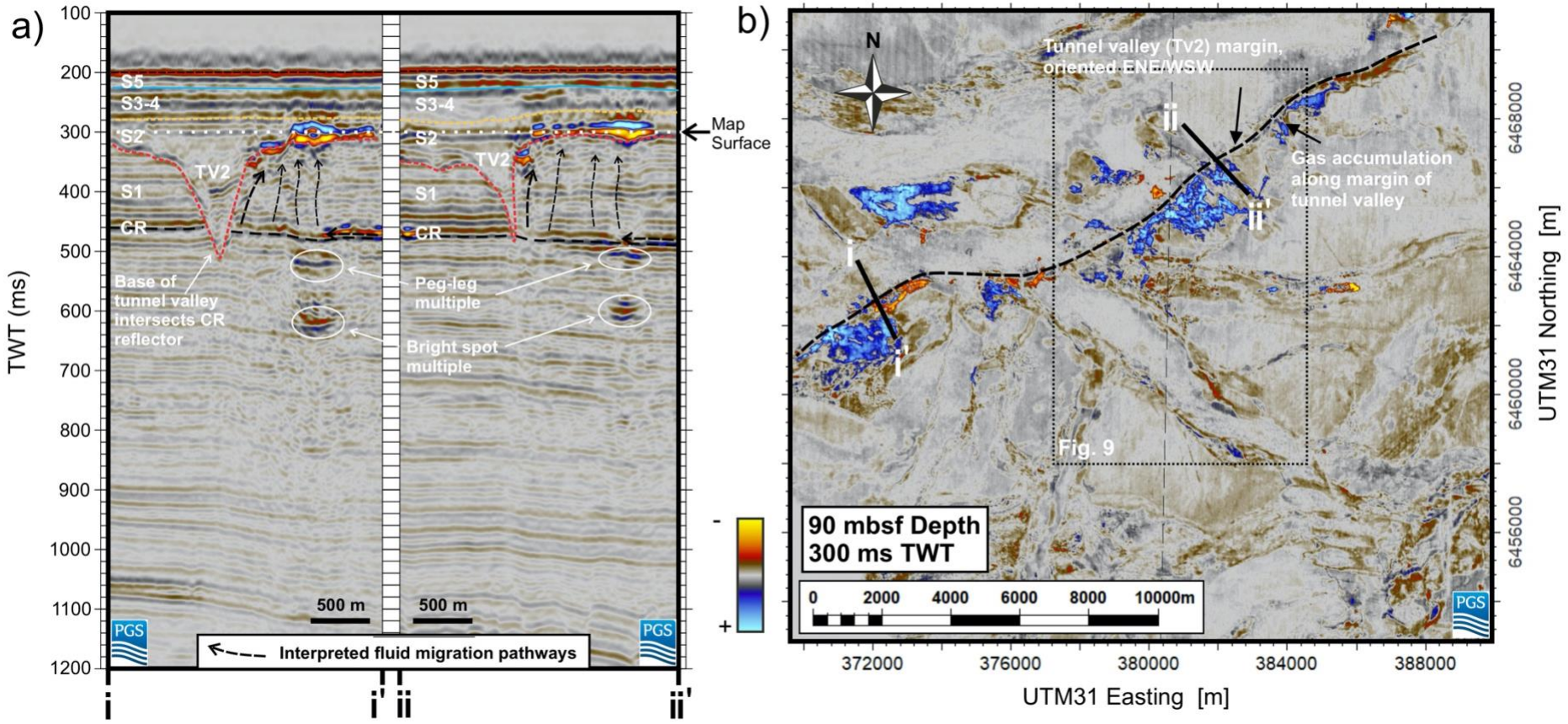

Figure 8. **Seismic interpretation and mapping of gas accumulation along the margin of a glacial tunnel valley at the Scanner pockmark complex. a)** Annotated seismic profiles highlighting interpreted fluid migration pathways from reflector CR to top of unit S2; **b)** Amplitude map at 90 metres below seafloor depth from 3D seismic reflection data, displaying the lateral extent and azimuth of high amplitude zones (blue). Black dashed box highlights the area shown in Fig. 9.

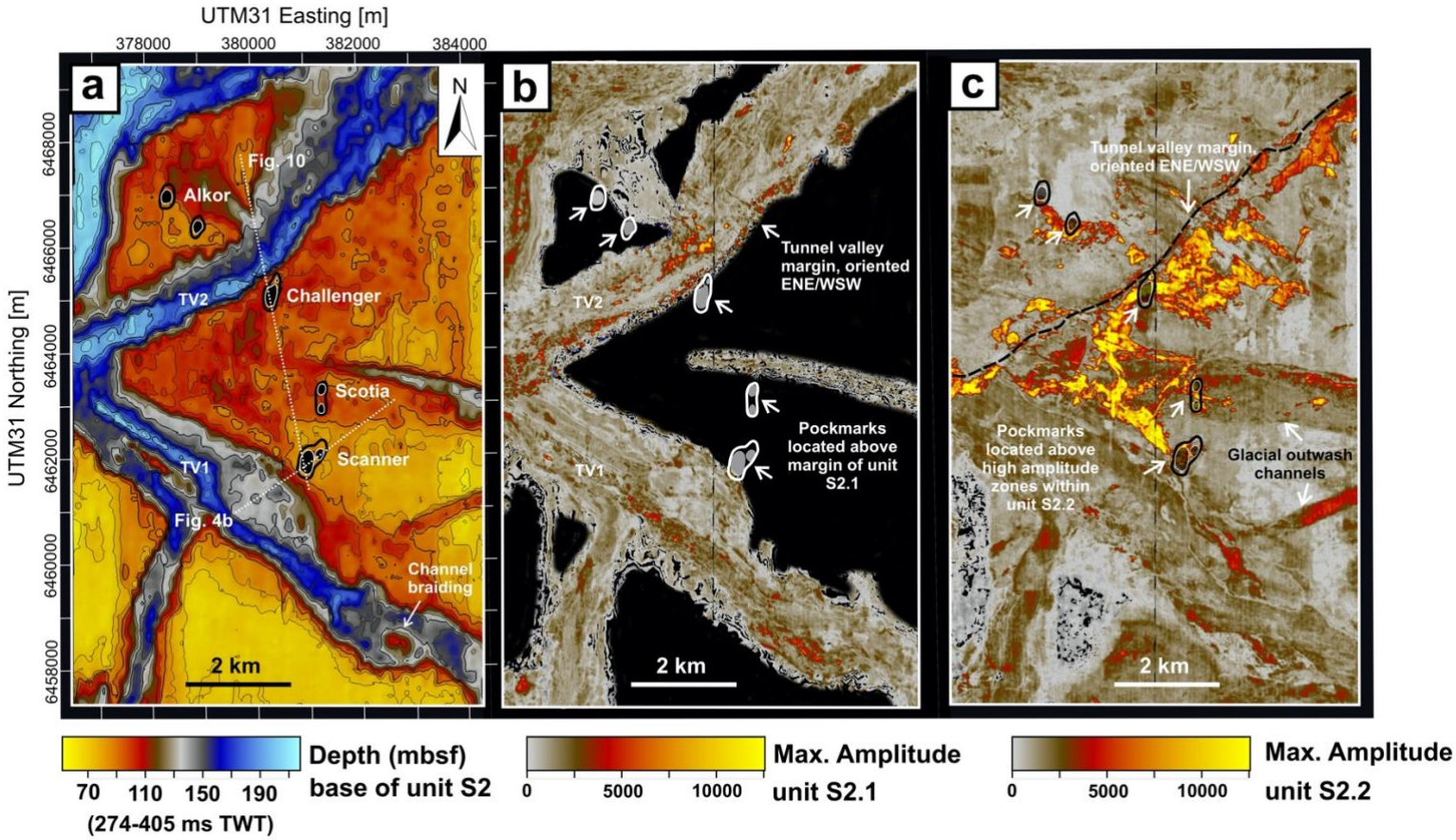

Figure 9. Glacial erosional features at base of the Ling Bank Fm. (a) Base of reflector S2 depth, **(b)** S2.1 maximum amplitude map, and **(c)** S2.2 maximum amplitude map from the 3D seismic reflection data, with windows of extraction over the full depth range of each unit. Gas has accumulated within the convergence of the glacial tunnel valleys TV1 and TV2, which act as a stratigraphic trap. Locations of the large pockmarks are displayed using a black/grey fill and black/white dotted outlines. Dotted white lines in a) show the locations of seismic data profiles shown in Fig. 4b and Fig. 10. The large pockmarks coincide with a) topographic highs, b) the margins of unit S2.1 and c) high amplitude zones within unit S2.2. TV – Tunnel valley.

4.1.3 Glacial erosional features – Ling Bank Fm.

Using the 3D seismic data, the base of the Ling Bank Fm. (S2) has been mapped, highlighting the topography of the erosional surface (Fig. 9). U-shaped glacial tunnel valleys have incised into the top of the Aberdeen Ground Fm (S1), are over 100 m deep and up to 1.5 km-wide, and represent a large stratigraphic discontinuity. Two tunnel valleys have converged, oriented NE/SW (TV2) and NW/SE (TV1). The base of TV2 intersects the CR surface (Fig. 8a). Within the Witch Ground Basin, the wider dominant flow direction of glaciers at the time of formation was North and West, as divergent ice flow sourced from the Norweigan Channel extended and terminated along the northern UK Atlantic continental margin (Graham et al. 2007; Ottesen et al. 2020). Therefore, the tunnel valleys observed at the Scanner pockmark complex site broadly correlate with the expected orientation. The large pockmarks (Scanner, Challenger and Alkor) are located proximal to the margins of the glacial channel features (Fig. 9b). Scotia pockmark appears to be an outlier, as is not located proximal to the tunnel valley margins. However, it is located adjacent to the deepest area of the glacial outwash channel, which extends to 130 mbsf (Fig. 9).

4.2 Gas spatial distribution

4.2.1 Gas accumulation – Ling Bank Fm.

Figure 9c displays the maximum seismic amplitude within the depth interval of unit S2.2 from the 3D seismic data. The presence of gas at this depth interval is interpreted from seismic amplitude maxima, sharp lateral amplitude cut-offs and polarity reversal along the reflection. Therefore, the spatial distribution of gas can be assessed within this unit. Gas is present beneath all of the large pockmarks (Fig. 9c). Gas appears to have been accumulated within the convergence of the two tunnel valleys (TV1-2; Fig. 9c; Judd et al. 1994; Böttner et al. 2019). It appears that gas is also concentrated and laterally constrained within the channelised features of seismic unit S2.2 (iii). Combining our seismic observations with understanding of North Sea glacial stratigraphy (Kluiving et al. 2003; Graham et al. 2006), we interpret the gas-charged sediments of unit S2.2 (iii) as coarse sands, sourced from a glacial outwash fan (Fig. 3; Kluiving et al. 2003; Graham et al. 2006). Further, unit S2.2 (iii) likely represents

a sandstone reservoir for methane gas accumulation, laterally constrained by clay sediments of unit S2.2 (ii) and vertically by unit S3. Assuming a thickness range of 10-30 m for unit S2.2 (iii) (calculated from an isochore thickness map, created from the depth-converted 3D seismic volume), an area of 6.43×10^6 m^2, corresponding to the amplitude maxima within unit S2.2 (iii) (Fig. 9c; amplitudes >5000; Supplementary Fig. S1) and a gas saturation range of 15-35 % (Gehrmann et al., 2021), we estimate a gas volume within the range of 9.65×10^6 to 6.75×10^7 m^3 for the reservoir. Based on an average annual seabed temperature of 7°C (Shell UK Limited, 2014), geothermal gradient of 30°C/km (Harper, 1971), seabed depth of 150 m and a 70-100 mbsf depth range of unit S2.2, an average CH_4 density of 17 kg/m^3 is calculated. Therefore, the total mass of CH_4 is estimated to range between 1.64×10^8 to 1.15×10^9 kg (0.16 to 1.15 MT) for the reservoir.

4.3 Shallow structural features

4.3.1 Shallow structural features – Coal Pit, LGM and Witch Ground Fms.

High-resolution surface sparker seismic reflection data provide a more detailed understanding of the shallow structure beneath the Scanner and Challenger pockmarks, down to a depth of 300 mbsf (450 ms TWTT). Fig. 10a displays a sparker seismic profile oriented N-S, which traverses these pockmarks. RMS amplitude sections reveals sub-vertical, high-amplitude, linear features at the top of unit S2.2 in the interpreted gas-saturated layers beneath the Scanner and Challenger pockmarks (Fig. 10b-c). The average horizontal spacing of these features is >10 m. The feature spacing is at least one order of magnitude greater than the calculated horizontal (2 m) and vertical (0.425 m) resolution of the seismic data at this depth interval. Analysis of the sparker profiles reveals no preferential orientation of the high amplitude lineations. The high amplitude features highlighted by the RMS amplitude sections are interpreted as fragmented gas saturated zones beneath the pockmarks at the top of unit 2.2 and of gas pockets extending into unit S3, which could be interpreted as a fracture damage zone. Immediately below the large pockmarks, the interpreted gas-filled fracture zones extend vertically upwards into unit S3 between 50-70 mbsf, in contrast with the surrounding gas saturated intervals of unit S2.2 (Fig. 10). This indicates that active fluid flow occurs from unit S2.2, upwards towards the base of the pockmarks,

through a zone of fractures. Sparker data also reveal seismic bright spots at the base of the Scanner (Fig. 11) and Challenger (Fig. 12) pockmarks, located within unit S4. We attribute the bright spots to gas accumulation within this unit, as well as the presence of methane-derived authigenic carbonates.

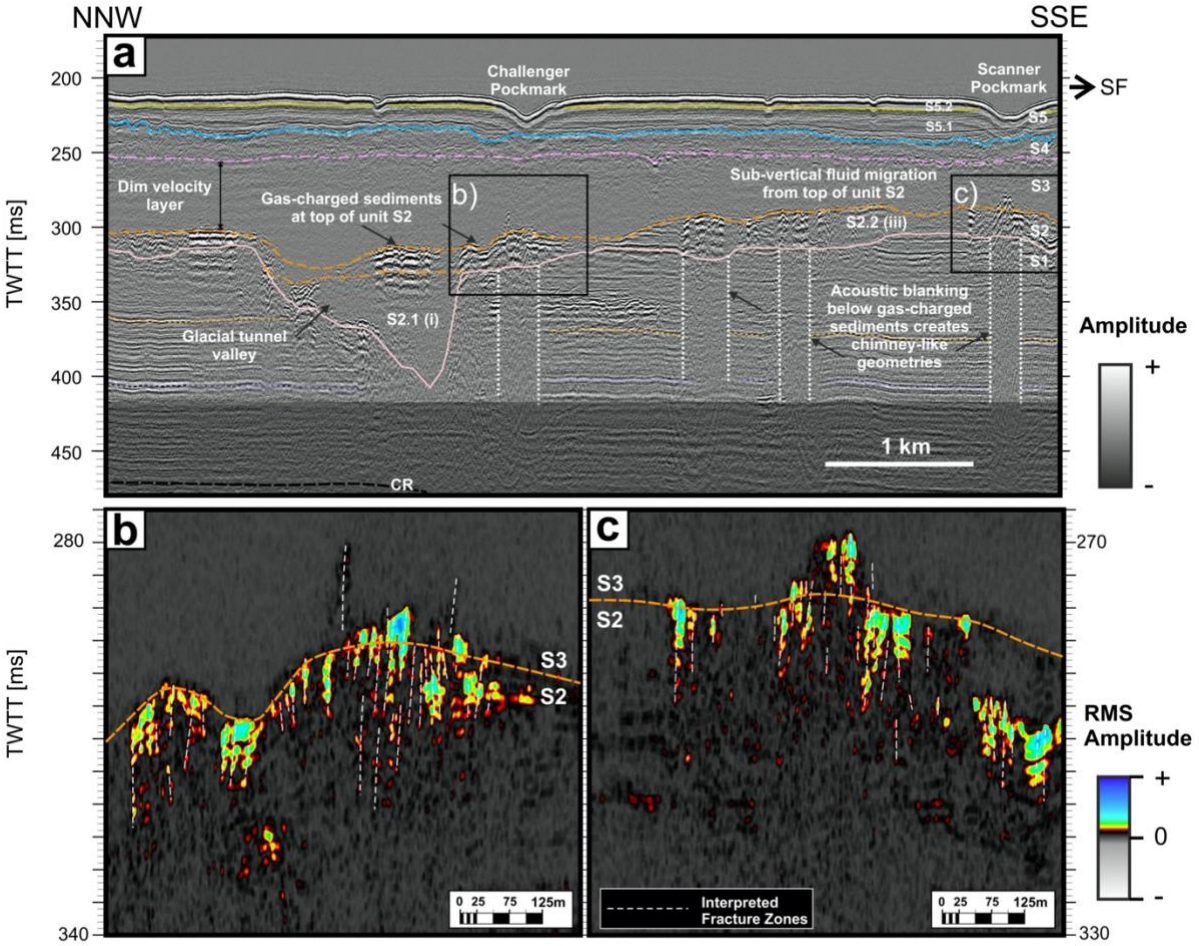

Figure 10. Sparker seismic reflection images of gas charged sediment and interpreted fracture zones within unit S2.2 (iii). (a) Profile across Challenger and Scanner pockmarks (position shown in Figs. 2 and 9). The colours of the reflectors are described in Fig. 4. Black boxes highlight the areas shown in b-c). **(b-c)** RMS amplitude profiles below b) Challenger and c) Scanner pockmarks. Interpreted gas-filled fracture zones (white dashed lines) are observed beneath the pockmarks at the top of unit S2 (Ling bank Fm.), extending into unit S3 (Coal Pit Fm.).

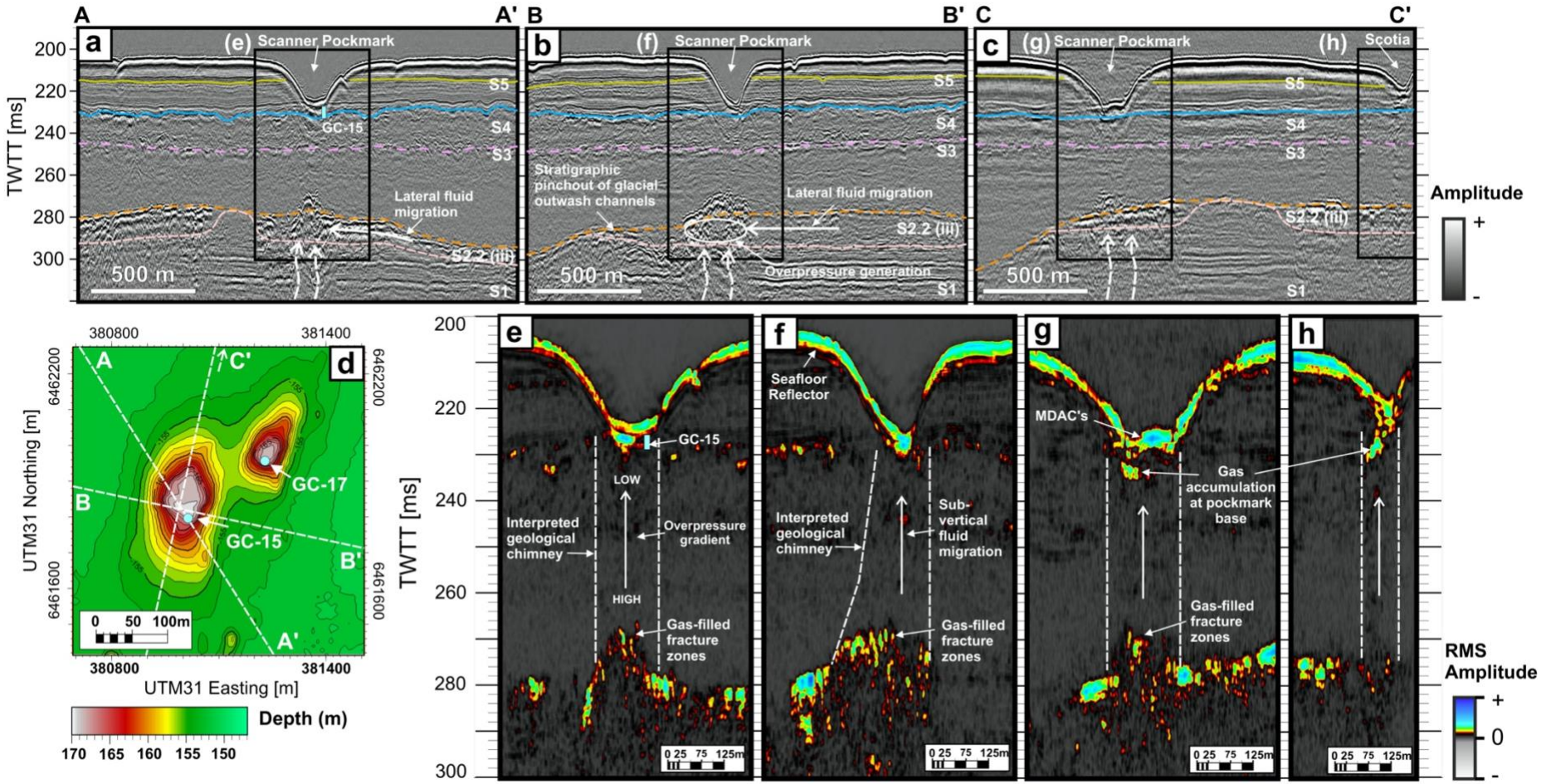

Figure 11. Sparker seismic reflection images of Scanner pockmark. (a-c) A stratigraphic pinch-out of glacial outwash channel sediments creates a stratigraphic trap, which generates fluid overpressure within unit S2.2(iii) directly below Scanner pockmark, leading to the formation of a gas chimney. The colour of the reflectors are as described in Figure 4. Black boxes highlight the areas of (e-h). Position of profile lines A, B and C are shown on **(d)** the bathymetry map. **(e-h)** show RMS profiles below Scanner pockmark.

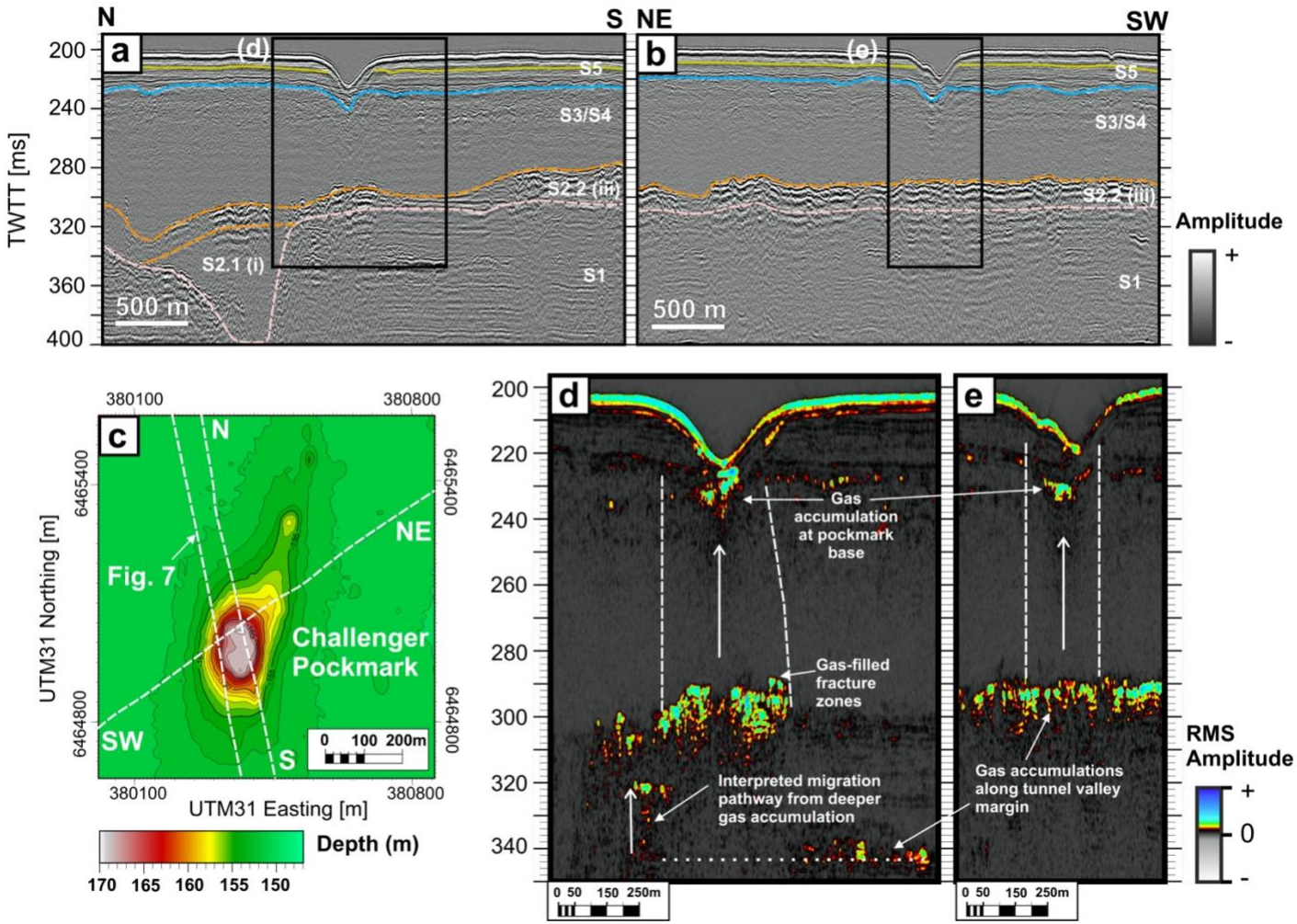

Figure 12. Sparker seismic reflection imaging of Challenger pockmark. (a-b) Vertical migration and accumulation of gas adjacent to the glacial tunnel valley is interpreted as a primary cause of fluid overpressure generation within unit S2.2 (iii), directly below Challenger pockmark, leading to the formation of a gas chimney. The colours of the reflectors are as described in Figure 4. Black boxes highlight the areas of (d-e). Position of profile lines N/S and NE/SW are shown on **(c)** the bathymetry map. **(d-e)** show RMS profiles below Challenger pockmark.

4.4 Sediment core analysis

Gravity cores extracted from below West (GC-15) and East (GC-17) Scanner pockmark (Figs. 2b and Supplementary Fig. S2) are composed of silty clay. The grain size distribution is highly uniform within the top 5 m, comprising 90-95 % clay, 2-8 % silt and 2-8 % fine sand. The gravity cores represent material extracted from units S4/S3 (LGM deposits and Coal Pit Formation). The uniformity of the grain size may partially explain the lack of acoustically prominent seismic reflectors within these respective units.

A sub-section of gravity core GC-17 from 3.5-4.0 mbsf was assessed using 3D X-ray micro-CT (XCT) imaging, which revealed the presence of disseminated iron sulphide (FeS) precipitation along slightly coarser-grained (fine sand) intervals (Fig. 13). Core evidence also reveals the presence of sediment remobilisation/fluidisation features, which are interpreted as in-situ features and may be attributed to fluid-escape (Fig. 13b; Supplementary Figure S2). In contrast to the sparker seismic reflection data, no sub-vertical fractures were observed from the gravity core data (Fig. 13b; Supplementary Fig. S2). The physical properties of the sediment cores are further described by Gehrmann et al. (2021), which calculate a modelled porosity decrease in the top 150 mbsf from 50 % (± 10%) to 25 % (± 3 %) due to sediment compaction. These porosities help facilitate the mass of methane accumulated in the shallow Ling Bank reservoir described in Section 4.2.

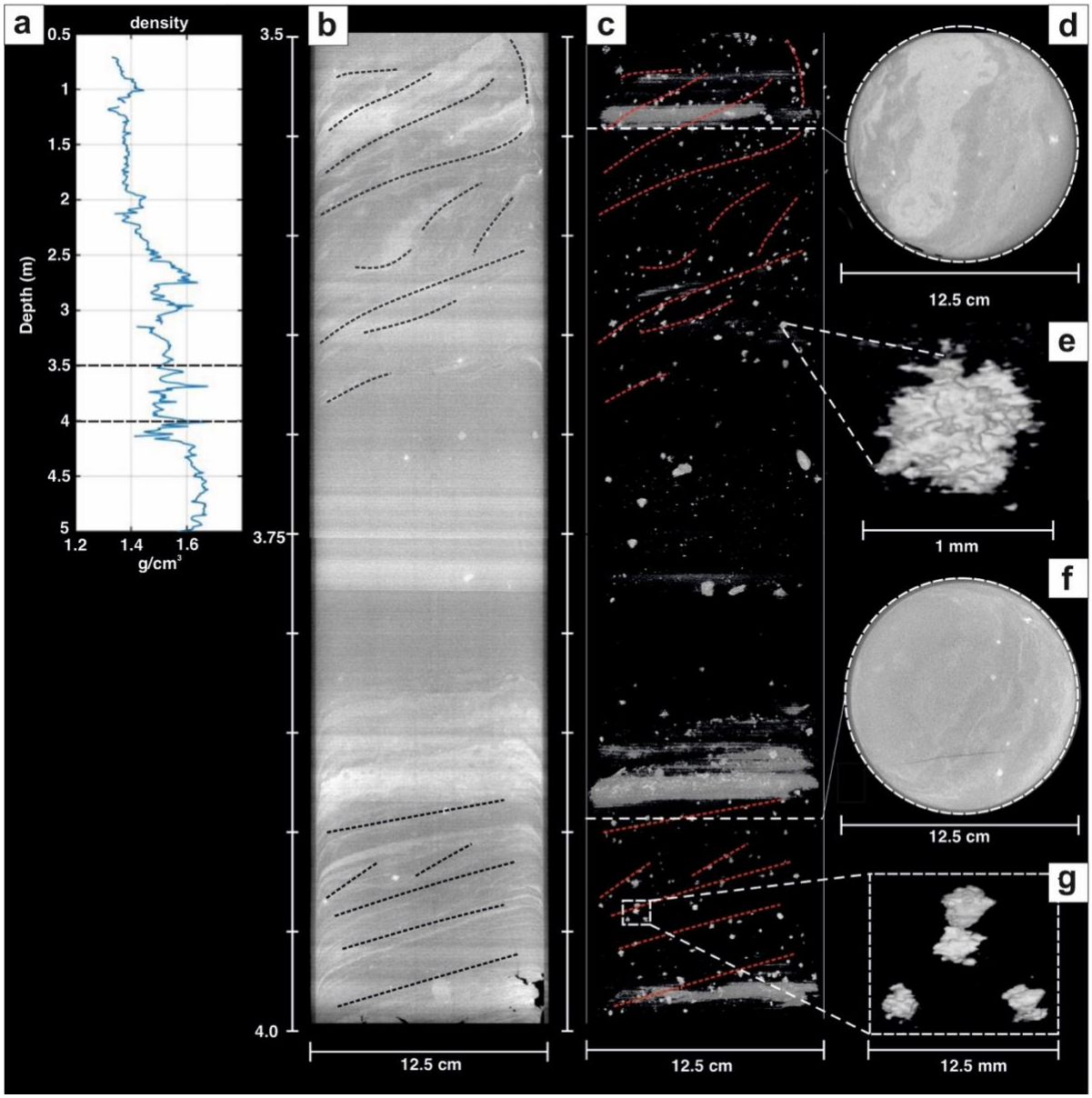

Figure 13. Gravity sediment cores recovered from below East Scanner pockmark (GC17; Fig. 2b, 4a and 11d) during the MSM78 expedition. The cores were analysed using (a) Multi-Sensor Core Logging (MSCL), which includes density data and (b-g) X-ray micro-CT analysis. (b), (d) and (f) Analysis of a 50 cm length x 12.5 cm diameter core section composed of clay and fine silt. Coarser-grained horizons (lighter grey) show evidence of fluidisation structures and layering, picked out by the dotted lines. (c) Same image as (b) but with lower density material removed, showing the presence of disseminated iron sulphide (bright spots, close-ups shown in e) and g) that has precipitated within the coarser grained horizons. The presence of iron sulphide is indicative of transport of methane-rich fluids through the coarser grained sediment horizons. Figure after Robinson et al. (2021).

5 Discussion

5.1 Migration pathways

From the seismic reflection imaging, a major gas saturated horizon has been identified based on the presence of high amplitude bright spots with reverse polarity and sharp lateral amplitude cutoffs; 1) the upper Ling Bank Fm. (S2.2; upper reservoir) at ~70 mbsf (300 ms TWTT). A hydraulic connection has also been interpreted between the upper Ling Bank Fm. and the Crenulate Reflector (CR) at ~270 mbsf (500 ms TWTT), which may be interpreted as a lower reservoir. In sedimentary basins, fluid flow and migration takes place preferentially through higher permeability pathways. Figure 14 shows the depth of maximum amplitude within the range of 55-135 mbsf (265-350 ms TWTT), that covers the depth range of the upper (S2) reservoir. Maximum amplitudes may correlate to areas of gas-saturated horizons (max. amplitudes >4000 – bright areas of Fig. 14; Supplementary Fig. S3). Maximum amplitudes may also correlate to high impedance contrasts created by lithological changes from clay-rich to sand-rich sediment layers (max amplitudes <4000 – dark areas of Fig. 14; Supplementary Fig. S3). Therefore, the map permits the identification of preferential fluid migration pathways in the sedimentary overburden along sand-rich, partially gas-saturated glacial outwash channels (Fig. 14).

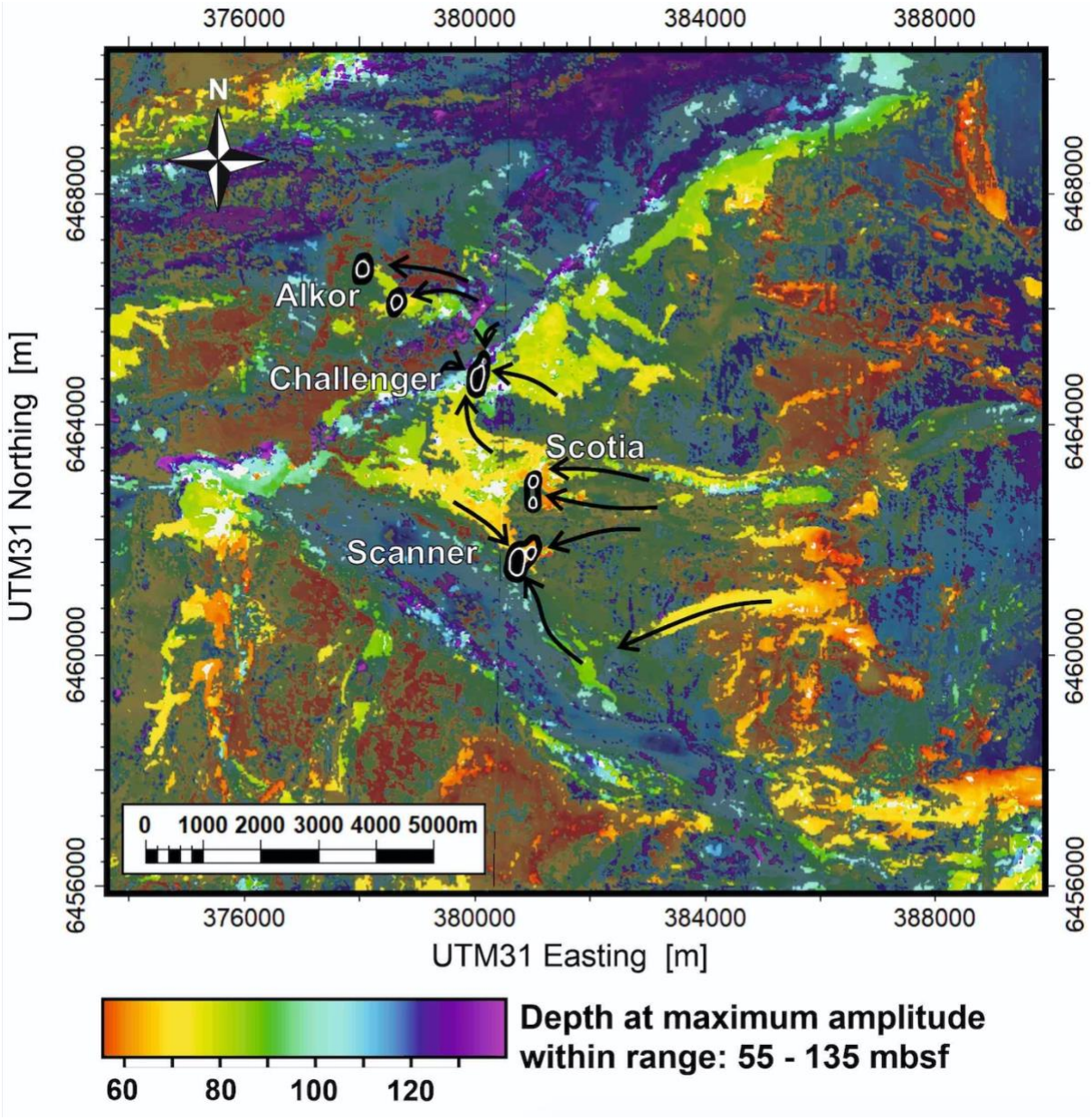

Figure 14. Distribution of gas-charged sediment across the Scanner pockmark complex from attribute analysis of 3D seismic reflection data. The map shows the depth to the maximum amplitude in the depth range 55-135 metres below seafloor. The time window of extraction is 85 ms (265-350 ms). Maximum amplitude is interpreted to correlate with the depth of gas charged sediment, as well as high impedance contrasts between clay-rich to sand-rich sediment. Therefore, the figure highlights the primary fluid migration pathways through glacial outwash channel sediments, which charge the shallow reservoir. Brighter areas represent amplitude maxima corresponding to gas-saturated sediment (seismic amplitudes > 4000). Black arrows indicate primary flow pathways towards the base of the large pockmarks. Locations of the large pockmarks are displayed using a black fill and dotted outlines.

At the Scanner pockmark complex, two types of fluid migration pathway are identified; 1) structurally-controlled fault and fracture pathways, and 2) stratigraphic pathways, including capillary flow through

high permeability sediment. The gas that emanates from the Challenger and Alkor pockmarks derives predominantly from structural pathways that are adjacent to the tunnel valley TV2, oriented ENE/WSW (Figs. 9 and 14). Gas is shown to have migrated upwards from more than 120 mbsf to less than 90 mbsf depth (Fig. 14; blue/purple to green/yellow). In contrast, the gas sourcing the Scotia and Scanner pockmarks more likely migrated along the glacial outwash fan channels, at depths less than 90 mbsf (Fig. 14; green to red). These glacial outwash fans represent zones of high permeability, which favours lateral gas migration from east to west, which correlates with the increase in seismic amplitude westwards towards the convergence of the tunnel valleys TV1 and TV2. Hence, we find that gas migration sourcing the large pockmarks is both structurally and stratigraphically controlled at the Scanner pockmark complex. This finding highlights the importance of considering lateral/horizontal gas flow as a source to the pockmarks and focused fluid conduits, which contrasts with models where gas migration is considered only to occur from directly below (e.g. Marin-Moreno et al. 2019).

Acoustic blanking beneath accumulations of gas below Scanner pockmark prevents direct observation and conclusive interpretation of the structure between the upper reservoir (S2.2) and the CR at these locations (Figs. 7, 10). However, high-resolution sparker seismic reflection data do permit direct observation of the sediment structure between the top of the upper reservoir (S2.2) and the pockmark base (Fig. 10). From the sparker RMS amplitude profiles we interpret gas-filled fracture zones that extend into the overlying Coal Pit Fm. (unit S3; Fig. 10). The presence of vertical gas conduits directly beneath Scanner pockmark, with preferential orientations of 70° and 150° was further demonstrated by Bayrakci et al. (2021) using shear-wave splitting (SWS) seismic anisotropy analysis. Therefore, the data indicate that the shallow reservoir is actively supplying gas to the pockmark. The SBP and sparker data also show that gas accumulation and pooling occurs within unit S4 at the base of the pockmark (Fig. 4a; Bayrakci et al., 2021).

The observed tidal variation of gas fluxes (Li et al., 2020) is consistent with gas transport through fractures that open at low tide in response to reductions in confining pressure or changes of gas solubility (e.g. Baghbanan & Jing, 2008; Rutqvist, 2015; Römer et al., 2016). Shallow, clay-rich sediments in this region are prone to hydraulic fracturing as a result of small changes of confining

pressure, causing vertical effective permeability increases of up to two orders of magnitude (Falcon-Suarez et al., 2021). The laterally extensive, overpressured reservoir located within unit S2.2 ensures continuous pore fluid pressure communication to the base of the gas chimneys, ensuring that the upward pressure gradient is maintained (Figs. 11,12). Therefore, the data indicate that fracture-dominant flow from the shallow reservoir to the pockmark prevails during low tide at reduced confining pressure.

Gravity core analysis evidences sediment remobilisation structures, but no fracturing within the top 5 m below Scanner pockmark (Fig. 13). The effective stress conditions close to the seafloor favour capillary-dominant flow (Cathles et al., 2010). In addition, previous core analysis of Witch Ground basin sediments shows that sand:clay ratios are much lower at shallow depths (<20 mbsf), and therefore more prone to plastic deformation (Paul & Jobson, 1991). This increase in plasticity would explain both the lack of fractures and the presence of fluidisation features within the gravity cores. However, given the small diameter of the cores (~0.1 m) relative to the diameter of the Scanner pockmarks (> 75 m width and >250 m long), it is probable that if fractured sediment is present in the shallow subsurface (< 5 mbsf), it could have been missed by the core drilling. Therefore, the dominant flow regime at depths < 5 mbsf remains inconclusive based on our data.

The interpreted lower reservoir CR surface, represents a regional unconformity between Pliocene and Pleistocene sediments (Fig. 3). This horizon dips downwards to the southeast (Figs. 6-7). Basin-scale up-dip migration likely occured along this unconformable surface (Fig. 1b), which prevents drawing conclusions about the original gas source from the seismic volume analysed here. Previous geochemical analysis by Judd et al. (1994) shows that the gas sourcing Scanner pockmark is predominantly biogenic gas, with only a minor thermogenic component, while Clayton & Dando (1996) interpret a more mixed biogenic and thermogenic source. Direct observation of interpreted sand-filled channels within the CR surface (Fig. 6) further indicates that gas migration through discrete zones of enhanced permeability may facilitate regional-scale fluid migration from greater depths. Lateral breaks in the seismic continuity of the CR surface beneath the Challenger and Scanner pockmarks supports the interpretation that gas from the CR is contributing to the supply of the upper reservoir (Unit S2.2 (iii); Fig. 8a) and therefore, a connected shallow gas migration system is present.

The 2D and 3D seismic reflection data provides strong evidence that the lower reservoir (CR) of the Scanner pockmark Complex is in hydraulic connection with the shallow gas system and large seabed pockmarks. Determining whether active fluid migration pathways exist below CR is therefore essential for the assessment of future subsurface CO_2 storage sites in the Central North Sea, where seabed pockmarks are observed in abundance (Fyfe et al., 2003). Seismic reflection data analysis revealed the presence of polygonal faults at > 860 mbsf (950 ms TWTT), with one of the predominant orientations comparable to the regional principal horizontal stress (50-60°; Fig. 5). Although the seismic reflection images display breaks in the lateral continuity of reflections between R2 and R1 (Fig. 7a), the absence of hydrocarbon indicators (DHI's) adjacent to the polygonal faults (Fig. 7), as well as the interpretation of seismic artefacts beneath the tunnels valleys and bright spots, suggests that the shallow gas migration system is not linked to these faults (Ho et al., 2018). Future seismic undershooting and reprocessing beneath the glacial tunnel valleys and shallow gas horizons may assist in more accurately resolving the stratigraphic and structural features of the layers between reflectors R2 and R1, as well as between reflectors CR and S2. This observation further indicates that an array of geophysical and geochemical methods are required to improve the characterisation of focused fluid conduits at the Scanner pockmark complex (Robinson et al., 2021).

5.2 Pockmark and chimney genesis

Several different mechanisms have been proposed to explain focused fluid conduit genesis, including erosive fluidisation, capillary driven invasion, fracture generation and reactivation (Lowe, 1975), localised subsurface volume loss and syn-sedimentary formation (Sun et al., 2013; Cartwright & Santamarina, 2015). However, when modelling focused fluid conduits, it is common to select one primary mechanism of genesis (e.g. Wangen, 2020). Integrating the seismic and sediment core observations from the Scanner pockmark complex, we develop an interpretation for focused fluid conduit and pockmark genesis, including temporal variability in response to changes in pore fluid pressure (Fig. 15):

1) Fluid overpressure is created within a shallow sandstone reservoir (unit S2.2 (iii)), comprised of glacial outwash channel sediments.
2) The reservoir pore-fluids are stratigraphically trapped within the convergence of a glacial tunnel valley, laterally constrained by the clay sediments of unit S2.2 (ii) and sealed by the overlying units S3-5. Pore-pressure increases inside the reservoir, caused by the migration and charge of pore-fluids along the glacial outwash channels towards the trap (Fig. 14).
3) At a critical fluid overpressure, whereby the pore pressure exceeds lithostatic pressure and the formation fracture pressure, hydraulic fractures are generated within units S3/S4 that extend to the base of S5.
4) Gas accumulates at the base of the Witch Ground Formation (base of unit S5), and once a critical overpressure is reached here, erosive fluidisation results in a blow-out event, displacing the Witch Ground sediments. Further, the exact location of gas accumulations beneath unit S5, and the consequent formation of large pockmarks, are likely controlled by the local surface topography of the base of unit S5 (see supplementary Fig. S4a). In addition, the blow out events are taking place where the overburden has the lowest thickness relative to the shallow gas reservoir in unit S2.1 (see supplementary Fig. S4b).
5) Once the pockmark has formed and the overpressure has reduced, capillary-dominant seep flow is likely to be the main flow mechanism from the base of the pockmark. Finally, cyclical, episodic fracture-dominant flow likely takes place during tidal-controlled reductions in confining pressure/effective stress.

After chimney genesis, fluid flow through a chimney may vary temporally in response to changes in pore fluid pressure, observed over shorter timescales as pulsed flow (Fig. 15). Transitions between capillary-dominant and fracture-dominant flow were also proposed by Roche et al. (2021) and Cevatoglu et al (2015) during controlled gas release experiments. Understanding temporal variations of fluid migration through focused fluid conduits is critical for subsurface CO_2 storage assessments.

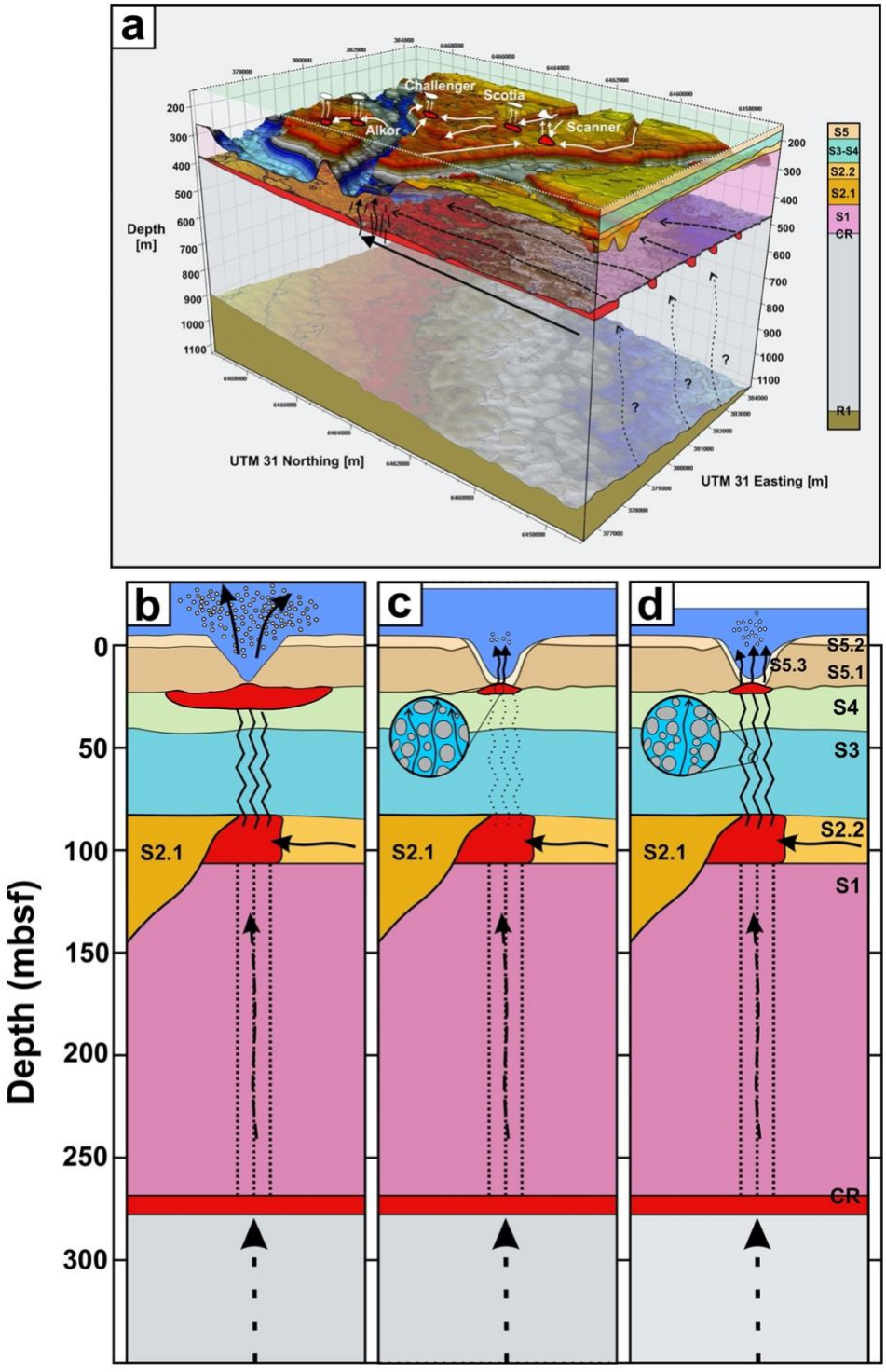

572

573 **Figure 15.** Temporal evolution and mechanisms of pockmark genesis and chimney formation. **(a)** 3D
574 seismic volume (depth converted) showing migration pathways that led to focusing of gas and
575 overpressure generation. **(b-c)** Schematic diagrams showing temporal evolution. **(b)** Erosive
576 fluidisation - initial blow-out and pockmark formation, release of overpressure in shallow reservoir,
577 preferential pathways established. **(c)** Seep flow - long term capillary flow from gas pooling at base of
578 pockmark. **(d)** Episodic pulsed flow - cyclical fracture flow from a shallow reservoir during periods of
579 reduced confining pressure, controlled by tidal current variations. mbsf – metres below seafloor.

5.3 Chimney seismic interpretation uncertainties and implications

Vertical seismic anomalies observed on seismic reflection data are commonly interpreted as focused fluid conduits. However, seismic artefacts, including acoustic blanking, bright spot multiples and velocity pull-up and pull-down effects can also generate vertical seismic anomalies, which can be misinterpreted as focused fluid conduits. For example, from the 2D sparker data in this study, acoustic blanking was observed beneath the gas-charged sediments of the shallow reservoir (unit S2.2; Fig 10). This acoustic blanking creates apparent chimney-like geometries beneath areas of higher gas-saturation (Fig. 10). Without data from lower frequency seismic sources, the blanking could have been misinterpreted as a gas chimney. In addition, bright-spot multiples, as well as velocity pull-up and pull-down effects were observed on the 3D seismic data, which if not correctly identified, may be misinterpreted as focused fluid conduits extending to depth intervals below the CR reflector (Fig. 7a). By omitting seismic artefacts from our geological interpretation, a real, physical chimney (i.e. a cylindrical column of gas-charged sediment) has only been unequivocally proven to occur from the seabed to the depth of the shallow reservoir at 90 mbsf. Therefore, we recommend that vertical seismic anomalies must be assessed with a site-specific approach, and put into a regional, geological context, and should not always be assumed to represent focused fluid conduits. This observation has important implications for assessments of the role of seismic chimneys in fluid flow for subsurface storage applications (Robinson et al., 2021).

6 Conclusions

In this study we have used high resolution 2D and 3D seismic reflection data to characterise an active fluid-escape system in the Witch Ground Basin, North Sea. Overall, the study has provided an improved understanding of focused fluid conduit process mechanisms, genesis, and temporal evolution. Based on the work presented, the following conclusions have been obtained.

A study of the regional-scale geology reveals that focused fluid conduits do not always represent a simplified cylindrical column of gas-charged sediment, sourced from directly below the structure. Instead, conduits may be fed from multiple depth intervals, including significant lateral migration of gas.

Within the overburden, the generation of overpressurised pore fluid required to form focused fluid conduits can be both structurally and stratigraphically controlled. In this study area, a shallow gas accumulation was laterally trapped within the convergence of two glacial tunnel valleys and vertically sealed by low permeability sediments.

The chimneys underlying the large pockmarks comprise a series of sub-vertically oriented gas-filled fracture zones. Gas-filled fracture zones are observed to extend vertically upwards from a shallow gas reservoir at <70 mbsf.

The seismic manifestation and interpretation of gas chimneys must be distinguished from seismic artefacts (false shallow signatures), which include acoustic blanking, bright spot multiples and chaotic reflections, to ensure that gas chimney presence and maximum depth extent is assessed correctly. This has important implications for assessments of subsurface storage containment integrity.

Data Availability

The datasets generated/analysed for this study can be found on Pangaea (Ref: PDI-27104). The 3D seismic data is available through the PGS data library (https://www.pgs.com/data-library/europe/nw-europe/north-sea/cns).

Acknowledgements

This work has received funding from the European Union's Horizon 2020 research and innovation programme under grant agreement No.654462 (STEMM-CCS) and the Natural Environment Research Council (CHIMNEY; NERC Highlight Topic; NE/N016130/1). We would like to thank all those involved in the planning and acquisition of data during research cruises JC152 (*RRS James Cook* cruise 152) and MSM78, including the officers, engineers and crews, the scientific parties, and all seagoing technicians and engineers. We are also grateful for the support of Applied Acoustics Ltd. during Sparker data acquisition. We acknowledge PGS for the use of their dataset. We thank Schlumberger for the donation of the Petrel 2019 software used for the seismic interpretation.

References

ACT Acorn Consortium. (2018). D08 East Mey CO2 Storage Site Development Plan 10196ACTC-Rep-26-01. https://www.actacorn.eu/sites/default/files/ACT%20Acorn%20East%20Mey%20CO2%20Storage%20Site%20Storage%20Development%20Plan%201.0_0.pdf.

Ahmadi, Z. M., Sawyers, M., Kenyon-Roberts, S., Stanworth, C. W., Kugler, K. A., Kristensen, J. & Fugelli, E. M. G., 2003. Paleocene. In: Evans, D., Eds., *The millennium atlas: Petroleum geology of the central and northern North Sea*, Geological Society of London, 235-259.

Alcalde, J., Heinemann, N., Mabon, L., Worden, R. H., De Coninck, H., Robertson, H., Maver, M., Ghanbari, S., Swennenhuis, F., Mann, I., …& Murphy, S. 2019. Acorn: Developing full-chain industrial carbon capture and storage in a resource- and infrastructure-rich hydrocarbon province. Journal of Cleaner Production, 233, 963-971, doi: 10.1016/j.jclepro.2019.06.087.

Andresen, K. J., 2012. Fluid flow features in hydrocarbon plumbing systems: What do they tell us about the basin evolution?. *Marine Geology*, **332**, 89-108, doi: 10.1016/j.margeo.2012.07.006.

Andrews, I. J., Long, D., Richards, P. C., Thomson, A. R., Brown, S., Chesher, J. A. & McCormac, M., 1990. *The geology of the Moray Firth* (Vol. 3). HMSO, London. http://pubs.bgs.ac.uk/publications.html?pubID=B01844.

Bachu, S., 2000. Sequestration of CO_2 in geological media: criteria and approach for site selection in response to climate change. *Energy conversion and management*, **41(9)**, 953-970, doi: 10.1016/S0196-8904(99)00149-1.

Baghbanan, A. & Jing, L., 2008. Stress effects on permeability in a fractured rock mass with correlated fracture length and aperture. *International Journal of Rock Mechanics and Mining Sciences*, **45(8)**, 1320-1334, doi: 10.1016/j.ijrmms.2008.01.015.

Bayrakci G., Callow B., Bull J. M., Minshull T. A., Provenzano G., North L., Macdonald C., Robinson A. H., Henstock T. & Chapman, M. (2021) Seismic anisotropy within an active fluid flow structure: Scanner Pockmark, North Sea. *Frontiers in Earth Science*, 9:626416, doi: 10.3389/feart.2021.626416.

Benson, S. M. & Cole, D. R., 2008. CO_2 Sequestration in Deep Sedimentary Formations. *Elements*, **4**, 325-331, doi: 10.2113/gselements.4.5.325.

659 Boldy, S. A. R., and Brealey, S. 1990. Timing, nature and sedimentary result of Jurassic tectonism in the
660 Outer Moray Firth. In: Hardman, R. F. P. & Brooks, J., Eds.,*Tectonic events responsible for Britain's*
661 *oil and gas reserves*. *Special Publication of the Geological Society of London*, **55**, 259-279, doi:
662 10.1144/GSL.SP.1990.055.01.12.
663 Böttner, C., Berndt, C. , Reinardy, B. T., Geersen, J., Karstens, J., Bull, J. M., Callow, B. J., Lichtschlag,
664 A., Schmidt, M., Elger, J., Schramm, B. & Haeckel, M., 2019. Pockmarks in the Witch Ground Basin,
665 Central North sea, *Geochemistry, Geophysics, Geosystems*, **20(4)**, 1698-1719.
666 Böttner, C., Haeckel, M., Schmidt, M., Berndt, C., Vielstädte, L., Kutsch, J. A., Karstens, J. & Weiß, T.,
667 2020. Greenhouse gas emissions from marine decommissioned hydrocarbon wells: leakage detection,
668 monitoring and mitigation strategies. *International Journal of Greenhouse Gas Control* **100**, doi:
669 10.1016/j.ijggc.2020.103119.
670 Bull, J. M., 2017. Cruise report – RRS James Cook JC152: CHIMNEY - Characterisation of major
671 overburden pathways above sub-seafloor CO_2 storage reservoirs in the North Sea. Scanner and
672 Challenger Pockmark Complexes. https://eprints.soton.ac.uk/420257/.
673 Bull, J. M., Berndt, C. B., Minshull, T. M., Henstock, T., Bayrakci, G., Gehrmann, R., Provenzano, G.,
674 Böttner, C., Schramm, B, Callow, B., …& Best, A. I., 2018. Constraining Leakage Pathways Through
675 the Overburden Above Sub-Seafloor CO_2 Storage Reservoirs. *14th Greenhouse Gas Control*
676 *Technologies Conference Melbourne 21-26 October 2018 (GHGT-14)*.
677 Bünz, S., Mienert, J. & Berndt, C., 2003. Geological controls on the Storegga gas-hydrate system of the
678 mid-Norwegian continental margin. *Earth and Planetary Science Letters*, **209(3-4)**, 291-307, doi:
679 10.1016/S0012-821X(03)00097-9.
680 Cartwright, J. & Santamarina, C., 2015. Seismic characteristics of fluid escape pipes in sedimentary basins:
681 Implications for pipe genesis. *Marine and Petroleum Geology*, **65**, 126-140, doi:
682 10.1016/j.marpetgeo.2015.03.023.
683 Cartwright, J., Huuse, M. & Aplin, A., 2007. Seal bypass systems. *AAPG bulletin*, **91**, 1141-1166, doi:
684 10.1306/04090705181.

685 Cartwright, J., Kirkham, C., Foschi, M., Hodgson, N., Rodriguez, K. & James, D. 2021. Quantitative
686 reconstruction of pore-pressure history in sedimentary basins using fluid escape pipes. Geology, doi:
687 10.1130/G48406.1.
688 Cartwright, J., James, D. & Bolton, A., 2003, The genesis of polygonal fault systems: a review. *Geological*
689 *Society, London, Special Publications*, **216(1)**, 223-243, doi: 10.1144/gsl.Sp.2003.216.01.15.
690 Cathles, L. M., Su, Z. & Chen, D., 2010. The physics of gas chimney and pockmark formation, with
691 implications for assessment of seafloor hazards and gas sequestration. *Marine and Petroleum*
692 *Geology*, **27(1)**, 82-91, doi: 10.1016/j.marpetgeo.2009.09.010.
693 Cevatoglu, M., Bull, J. M., Vardy, M. E., Gernon, T. M., Wright, I. C. & Long, D., 2015. Gas migration
694 pathways, controlling mechanisms and changes in sediment acoustic properties observed in a
695 controlled sub-seabed CO_2 release experiment. *International Journal of Greenhouse Gas Control*. **38**,
696 26-43, doi: 10.1016/j.ijggc.2015.03.005.
697 Clayton, C. J. & Dando, P. R., 1996. Comparison of seepage and seal leakage rates. In: Schumacher, D.
698 & Abrams, M.A., Eds., *Hydrocarbon Migration and Its Near-surface Expression. In: Outgrowth of*
699 *the AAPG Hedberg Research Conference. American Association of Petroleum Geologists Memoir*,
700 Vancouver, British Columbia, April 24-28, 1994 (No. 66). AAPG.
701 Cole, D., Stewart, S. A. & Cartwright, J. A., 2000. Giant irregular pockmark craters in the Palaeogene of
702 the Outer Moray Firth Basin, UK North Sea. *Marine and Petroleum Geology*, **17**, 563-577, doi:
703 10.1016/S0264-8172(00)00013-1.
704 Copestake, P., Sims, A. P., Crittenden, S., Hamar, G. P., Ineson, J. R., Rose, P. T. & Tringham, M. E.,
705 2003. Lower Cretaceous. In: Evans, D., Eds., *The millennium atlas: Petroleum geology of the central*
706 *and northern North Sea, Geological Society of London*, 191-211.
707 Etiope, G., Ciotoli, G., Schwietzke, S. & Schoell, M., 2019a. Gridded maps of geological methane
708 emissions and their isotopic signature. *Earth System Science Data*, **11**, 1-22, doi: 10.5194/essd-11-1-
709 2019.
710 Etiope, G., Schwietzke, S., Helmig, D. & Palmer, P., 2019b. Global geological methane emissions: An
711 update of top-down and bottom-up estimates, *Elementa-Science Of The Anthropocene*, **7**, doi:
712 10.1525/elementa.383.

713 Evans, C. J. & Brereton, N. R., 1990. In situ crustal stress in the United Kingdom from borehole breakouts.
714 *Geological Society, London, Special Publications*, **48(1)**, 327-338, doi:
715 10.1144/gsl.Sp.1990.048.01.27.
716 Falcon-Suarez, I.H., Lichtschlag, A., Marin-Moreno, H., Papageorgiou, G., Sahoo, S.K., Roche, B.,
717 Callow, B., Gehrmann, R.A.S., Chapman, M., North, L., 2021. Core-scale geophysical and
718 hydromechanical analysis of seabed sediments affected by CO_2 venting. *International Journal of*
719 *Greenhouse Gas Control*, **108**, 103332, doi: 10.1016/j.ijggc.2021.103332.
720 Fauria, K. E. & Rempel, A. W., 2011. Gas invasion into water-saturated, unconsolidated porous media:
721 Implications for gas hydrate reservoirs. *Earth and Planetary Science Letters*, **312(1-2)**, 188-193, doi:
722 10.1016/j.epsl.2011.09.042.
723 Flohr, A., Schaap, A., Achterberg, E.P., Alendal, G., Arundell, M., Berndt, C., Blackford, J., Böttner, C.,
724 Borisov, S.M., Brown, R. and Bull, J.M., 2021. Towards improved monitoring of offshore carbon
725 storage: A real-world field experiment detecting a controlled sub-seafloor CO2 release. *International*
726 *Journal of Greenhouse Gas Control*, 106, p.103237.
727 Frahm, L., Hübscher, C., Warwel, A., Preine, J. & Huster, H., 2020. Misinterpretation of velocity pull-ups
728 caused by high-velocity infill of tunnel valleys in the southern Baltic Sea. *Near Surface Geophysics*,
729 doi:10.1002/nsg.12122.
730 Frey, S. E., Gingras, M. K & Dashtgard, S. E., 2009. Experimental studies of gas-escape and water-escape
731 structures: mechanisms and morphologies. *Journal of Sedimentary Research*, **79(11)**, 808-816, doi:
732 10.2110/jsr.2009.087.
733 Furre, A.-K., Eiken, O., Alnes, H., Vevatne, J. N. & Kiær, A. F. 2017. 20 Years of Monitoring CO2-
734 injection at Sleipner. *Energy Procedia*, **114**, 3916-3926, doi: 10.1016/j.egypro.2017.03.1523.
735 Fyfe, J. A., Gregersen, U., Jordt, H., Rundberg, Y., Eidvin, T., Evans, D., Stewart, D., Hovland, M. &
736 Andresen, P., 2003. Oligocene to Holocene. In: Evans, D., Eds., *The millennium atlas: Petroleum*
737 *geology of the central and northern North Sea*, Geological Society of London, 279-287.
738 Gafeira, J. & Long, D. 2015. Geological investigation of pockmarks in the Scanner Pockmark SCI area.
739 JNCC Report No 570. JNCC Peterborough. http://data.jncc.gov.uk/data/290b95b7-fcfc-4c76-8780-
740 8714329dcf0c/JNCC-Report-570-FINAL-WEB.pdf.

741 Gafeira, J., Long, D. and Diaz-Doce, D., 2012. Semi-automated characterisation of seabed pockmarks in
742 the central North Sea. *Near Surface Geophysics*, **10**(4), 301-312, doi: 10.3997/1873-0604.2012018.
743 Gay, A., Lopez, M., Berndt, C. & Séranne, M., 2007. Geological controls on focused fluid flow associated
744 with seafloor seeps in the Lower Congo Basin. *Marine Geology*, **244**, 68-92, doi:
745 10.1016/j.margeo.2007.06.003.
746 Gehrmann, R. A. S., Provenzano, G., Böttner, C. , Marn-Moreno, H., Bayrakci, G., Tan, Y. Y., Yilo, N.
747 K., Djanni, A. T., Weitemeyer, K. A., Minshull, T. A., Bull, J. M., Karstens, J. and Berndt, C. (2021)
748 Porosity and free gas estimates from controlled source electromagnetic data at the Scanner Pockmark
749 in the North Sea. *International Journal of Greenhouse Gas Control*, 109, 103343, doi:
750 10.1016/j.ijggc.2021.103343.
751 Global CCS Institute. (2020). Global status of CCS: 2020.
752 https://www.globalccsinstitute.com/resources/global-status-report/.
753 Graham, A., Lonergan, L. & Stoker, M., 2007. Evidence for Late Pleistocene ice stream activity in the
754 Witch Ground Basin, central North Sea, from 3D seismic reflection data. *Quaternary Science*
755 *Reviews*, **26(5-6)**, 627-643, doi: 10.1016/j.quascirev.2006.11.004.
756 Greinert, J., McGinnis, D. F., Naudts, L., Linke, P. & De Batist, M., 2010. Atmospheric methane flux from
757 bubbling seeps: Spatially extrapolated quantification from a Black Sea shelf area. *Journal of*
758 *Geophysical Research: Oceans*, **115 (C1)**, doi: 10.1029/2009JC005381.
759 Harper, M. L., 1971. Approximate geothermal gradients in the North Sea Basin. *Nature*, 230, 235-236,
760 doi:10.1038/230235a0.
761 Hindle, A. D., 1997. Petroleum Migration Pathways and Charge Concentration: A Three-Dimensional
762 Model. *AAPG Bulletin*; **81 (9)**: 1451–1481, doi: 10.1306/3B05BB1E-172A-11D7-
763 8645000102C1865D.
764 Ho, S., Hovland, M., Blouet, J.-P., Wetzel, A., Imbert, P. & Carruthers, D., 2018. Formation of linear
765 planform chimneys controlled by preferential hydrocarbon leakage and anisotropic stresses in faulted
766 fine-grained sediments, offshore Angola. *Journal of Geophysical Research: Solid Earth*, **1437(9)**,
767 1437–1468, doi: 10.5194/se-9-1437-2018.

768 Holmes, R. & Stoker, S.J., 2005. Investigation of the origin of shallow gas in outer Moray Firth open
769 blocks 15/20c and 15/25d. British Geological Survey, 34pp.
770 http://nora.nerc.ac.uk/id/eprint/11247/1/CR05030N.pdf
771 Hovland, M. & Sommerville, J. H., 1985. Characteristics of two natural gas seepages in the North Sea.
772 *Marine and Petroleum Geology*, **2(4)**, 319-326, doi: 10.1016/0264-8172(85)90027-3.
773 Hovland, M., Heggland, R., De Vries, M. H. & Tjelta, T. I., 2010. Unit-pockmarks and their potential
774 significance for predicting fluid flow. *Marine and Petroleum Geology*, **27**, 1190-1199, doi:
775 10.1016/j.marpetgeo.2010.02.005.
776 Hustoft, S., Bünz, S. & Mienert, J., 2010. Three-dimensional seismic analysis of the morphology and
777 spatial distribution of chimneys beneath the Nyegga pockmark field, offshore mid-Norway. *Basin*
778 *Research*, **22(4)**, 465-480, doi: 10.1111/j.1365-2117.2010.00486.x.
779 Judd, A. & Hovland, M., 2009. *Seabed fluid flow: the impact on geology, biology and the marine*
780 *environment*. Cambridge University Press, doi: 10.1017/CBO9780511535918.
781 Judd, A., Long, D. & Sankey, M., 1994. Pockmark formation and activity, UK block 15/25, North Sea,
782 *Bulletin of the Geological Society of Denmark*, **41**, 34-49.
783 Karstens, J. & Berndt, C., 2015. Seismic chimneys in the Southern Viking Graben – Implications for
784 palaeo fluid migration and overpressure evolution. *Earth and Planetary Science Letters*, **412**, 88-100,
785 doi: 10.1016/j.epsl.2014.12.017.
786 Karstens, J., Böttner, C., Edwards, M., Falcon-Suarez, I., Flohr, A., James, R., Lichtschlag, A., Maicher,
787 D., Pheasant, I., Roche, B., Schramm, B. & Wilson, M., 2019b. RV MARIA S. MERIAN Cruise
788 Report MSM78-PERMO2, Edinburgh–Edinburgh (UK), 16.10.-25.10.2018. doi:
789 10.3289/geomar_rep_ns_48_2019.
790 Karstens, J., Müller, P., Berndt, C. & Patruno, S., 2019a. Deep-seated focused fluid migration as indicator
791 for hydrocarbon leads in the East Shetland Platform, North Sea Province. *Geological Society, London,*
792 *Special Publications*, **494**, doi: 10.1144/SP494-2019-26.
793 Kluiving, S.J., Bosch, J.A., Ebbing, J.H., Mesdag, C.S. & Westerhoff, R.S., 2003. Onshore and offshore
794 seismic and lithostratigraphic analysis of a deeply incised Quaternary buried valley system in the

795 Northern Netherlands. *Journal of Applied Geophysics*, **53(4)**, 249-271, doi:
796 10.1016/j.jappgeo.2003.08.002.
797 Leifer, I. & Boles, J., 2005. Measurement of marine hydrocarbon seep flow through fractured rock and
798 unconsolidated sediment. *Marine and Petroleum Geology*, **22(4)**, 551-568, doi:
799 10.1016/j.marpetgeo.2004.10.026
800 Li, J., Roche, B., Bull, J.M., White, P.R., Leighton, T.G., Provenzano, G., Dewar, M. & Henstock, T.J.,
801 2020. Broadband Acoustic Inversion for Gas Flux Quantification—Application to a Methane Plume
802 at Scanner Pockmark, Central North Sea. *Journal of Geophysical Research: Oceans*, **125(9)**,
803 p.e2020JC016360.
804 Ligtenberg, H. & Connolly, D., 2003. Chimney detection and interpretation, revealing sealing quality of
805 faults, geohazards, charge of and leakage from reservoirs. *Journal of geochemical exploration*, **78** ,
806 385-387, doi: 10.1016/S0375-6742(03)00095-5.
807 Lloyd, C., Huuse, M., Barrett, B. J., Stewart, M. A. & Newton, A. M. W. 2021. A regional CO_2
808 containment assessment of the northern Utsira Formation seal and overburden, northern North Sea.
809 *Basin Research*, doi: 10.1111/bre.12545.
810 Løseth, H., Gading, M. & Wensaas, L., 2009. Hydrocarbon leakage interpreted on seismic data. *Marine*
811 *and Petroleum Geology*, **26(7)**, 1304-1319, doi: 10.1016/j.marpetgeo.2008.09.008.
812 Løseth, H., Wensaas, L., Arntsen, B., Hanken, N.-M., Basire, C. & Graue, K., 2011. 1000 m long gas
813 blow-out pipes. *Marine and Petroleum Geology*, **28(5)**, 1047-1060,
814 doi:10.1016/j.marpetgeo.2010.10.001.
815 Lowe, D. R., 1975. Water escape structures in coarse-grained sediments, *Sedimentology*, **22(2)**, 157-204,
816 doi: 10.1111/j.1365-3091.1975.tb00290.x.
817 Marin-Moreno, H., Bull J. M., Matter J., Sanderson, D. J. & Roche, B., 2019. Reactive transport modelling
818 insights into CO_2 migration through sub-vertical fluid flow structures. *International Journal of*
819 *Greenhouse Gas Control*, **86**, 82-92, doi: 10.1016/j.ijggc.2019.04.018.
820 Moss, J. L. & Cartwright, J., 2010a. 3D seismic expression of km-scale fluid escape pipes from offshore
821 Namibia. *Basin Research*, **22(4)**, 481-501, doi: 10.1111/j.1365-2117.2010.00461.x.

822 Moss, J. L. & Cartwright, J., 2010b. The spatial and temporal distribution of pipe formation, offshore
823 Namibia. *Marine and Petroleum Geology*, **27(6)**, 1216-1234, doi: 10.1016/j.marpetgeo.2009.12.013.
824 Nichols, R. J., Sparks, R. S. J. & Wilson, C. J. N., 1994. Experimental studies of the fluidization of layered
825 sediments and the formation of fluid escape structures. *Sedimentology*, **41(2)**, 233-253, doi:
826 10.1111/j.1365-3091.1994.tb01403.x.
827 Ottesen, D., Dowdeswell, J. A. & Bugge, T., 2014. Morphology, sedimentary infill and depositional
828 environments of the Early Quaternary North Sea Basin (56–62 N). *Marine and Petroleum Geology*,
829 **56**, 123-146, doi: 10.1016/j.marpetgeo.2014.04.007.
830 Ottesen, D., Stewart, M., Brönner, M. and Batchelor, C.L., 2020. Tunnel valleys of the central and northern
831 North Sea (56° N to 62° N): Distribution and characteristics. *Marine Geology*, 425, 106199, doi:
832 10.1016/j.margeo.2020.106199.
833 Paul, M. A. & Jobson, L. M., 1991. Geotechnical properties of soft clays from the Witch Ground Basin,
834 central North Sea. *Geological Society, London, Engineering Geology Special Publications*, **7(1)**, 151-
835 156, doi: 10.1144/gsl.Eng.1991.007.01.12.
836 Plaza-Faverola, A., Vadakkepuliyambatta, S., Hong, W. L., Mienert, J., Bünz, S., Chand, S. & Greinert,
837 J., 2017. Bottom-simulating reflector dynamics at Arctic thermogenic gas provinces: An example
838 from Vestnesa Ridge, offshore west Svalbard. *Journal of Geophysical Research: Solid Earth*, **122**,
839 4089-4105, doi: 10.1002/2016jb013761.
840 Provenzano, G., Henstock, T. J., Bull, J. M. & Bayrakci, G., 2020. Attenuation of receiver ghosts in
841 variable-depth streamer high-resolution seismic reflection data. *Marine Geophysical Research*, **41**, 1-
842 15, doi: 10.1007/s11001-020-09407-9.
843 Reinardy, B.T., Hjelstuen, B.O., Sejrup, H.P., Augedal, H., Jørstad, A.,(2017) Late Pliocene-Pleistocene
844 environments and glacial history of the northern North Sea. Quat. Sci. Rev., 158, 07-126,
845 doi:10.1016/j.quascirev.2016.12.022.
846 Ringrose, P. S., & Meckel, T. A. (2019). Maturing global CO2 storage resources on offshore continental
847 margins to achieve 2DS emissions reductions. *Scientific Reports*, **9**, 1–10, doi: 10.1038/s41598-019-
848 54363-z.

Robinson, A.H., Callow, B., Böttner, C., Yilo, N., Provenzano, G., Falcon-Suarez, I. H., Marin-Moreno, H., Lichtschlag, A., Bayrakci, G., Gehrmann, R., ...& Reinardy, B. (2021). Multiscale characterisation of chimneys/pipes: Fluid escape structures within sedimentary basins. *International Journal of Greenhouse Gas Control*, 106, 103245, doi: 10.1016/j.ijggc.2020.103245.

Robinson, A., Bayracki, G., MacDonald, C., Callow, B., Provenzano, G., Minshull, T., Chapman, M., Henstock, T., and Bull, J. 2020. Fracture characterisation using frequency-dependent shear-wave splitting analysis of azimuthal anisotropy: application to fluid flow pathways at the Scanner Pockmark area, North Sea, *EGU General Assembly 2020*, EGU2020-6669, doi: 10.5194/egusphere-egu2020-6669, 2020

Roche, B., Bull, J. M., Marin-Moreno, H., Leighton, T., Falcon-Suarez, I. H., White, P. R., Provenzano, G., Tholen, M., Lichtschlag, A., Li, J., & Faggetter, M. (2021). Time-lapse imaging of CO_2 migration within near-surface sediments during a controlled sub-seabed release experiment. *International Journal of Greenhouse Gas Control*, 109, 103363, doi: 10.1016/j.ijggc.2021.103363.

Römer, M., Riedel, M., Scherwath, M., Heesemann, M. & Spence, G. D., 2016. Tidally controlled gas bubble emissions: A comprehensive study using long-term monitoring data from the NEPTUNE cabled observatory offshore Vancouver Island. *Geochemistry, Geophysics, Geosystems*, **17**, 3797-3814, doi: 10.1002/2016GC006528.

Rutqvist, J., 2015. Fractured rock stress-permeability relationships from in situ data and effects of temperature and chemical-mechanical couplings. *Geofluids*, **15(1-2)**, 48-66, doi: 10.1111/gfl.12089.

Saunois, M., Stavert, A. R., Poulter, B., Bousquet, P., Canadell, J. G., Jackson, R. B., Raymond, P. A., Dlugokencky, E. J., Houweling, S., Patra, P. K., Ciais, P., ...& Zhuang, Q., 2020. The Global Methane Budget 2000–2017, *Earth System Science Data*, **12**, 1561-1623, doi: 10.5194/essd-12-1561-2020.

Schramm, B., Bayrakci, G., Dannowski, A., Böttner, C., Berndt, C., Henstock, T. J., Bull, J. and Minshull, T., 2019. Imaging the 3D seismic velocity structure of the Scanner pockmark, central North Sea. *AGU Fall Meeting 2019*, OS41B-1671.

Shakhova, N., Semiletov, I., Salyuk, A., Yusupov, V., Kosmach, D., & Gustafsson, Ö., 2010. Extensive methane venting to the atmosphere from sediments of the East Siberian Arctic Shelf. *Science*, **327 (5970)**, 1246-1250, doi: 10.1126/science.1182221.

877 Shell UK Limited, 2014. Peterhead CCS Project – Well Completion Concept Select Report PCCS-05-PT-
878 ZW-7180-00003.
879 Stewart, M. A., & Lonergan, L., 2011. Seven glacial cycles in the middle-late Pleistocene of northwest
880 Europe: Geomorphic evidence from buried tunnel valleys. *Geology*, **39(3)**, 283-286, doi:
881 10.1130/g31631.1.
882 Stoker, M.S., Balson, P.S., Long, D. & Tappin, D.R., 2011. *An overview of the lithostratigraphical*
883 *framework for the Quaternary deposits on the United Kingdom continental shelf*. Nottingham, UK,
884 British Geological Survey. http://nora.nerc.ac.uk/id/eprint/15939.
885 Sun, Q. L., Cartwright, J., Wu, S. G. & Chen, D. X., 2013. 3D seismic interpretation of dissolution pipes
886 in the South China Sea: Genesis by subsurface, fluid induced collapse. *Marine Geology*, **337**, 171-
887 181, doi: 10.1016/j.margeo.2013.03.002.
888 Taylor, P., Stahl, H., Vardy, M.E., Bull, J.M., Akhurst, M., Hauton, C., James, R.H., Lichtschlag, A., Long,
889 D., Aleynik, D. & Toberman, M., 2015. A novel sub-seabed CO_2 release experiment informing
890 monitoring and impact assessment for geological carbon storage. *International Journal of Greenhouse*
891 *Gas Control*, **38**, 3-17, doi: 10.1016/j.ijggc.2014.09.007.
892 Tóth, J., 1980. Cross-formational gravity-flow of groundwater: A mechanism of the transport and
893 accumulation of petroleum (the generalized hydraulic theory of petroleum migration). *Problems of*
894 *Petroleum Migration, AAPG*, 121-167, doi: 10.1306/St10411C8.
895 Wangen, M., 2020. A 3D model for chimney formation in sedimentary basins. *Computers & Geosciences*,
896 **137**, doi: 10.1016/j.cageo.2020.104429.
897 Watson, T. L. & Bachu, S., 2009. Evaluation of the Potential for Gas and CO_2 Leakage Along Wellbores.
898 *Society of Petroleum Engineers*, doi: 10.2118/106817-PA.
899 Zanella, E. & Coward, M. P., 2003. Structural framework. In: Evans, D., Eds., *The millennium atlas:*
900 *Petroleum geology of the central and northern North Sea*, Geological Society of London, 45-59.

Supplementary Material

Four supplementary figures (Figs. S1-S4) are provided for this article, which are also located in a separate file.

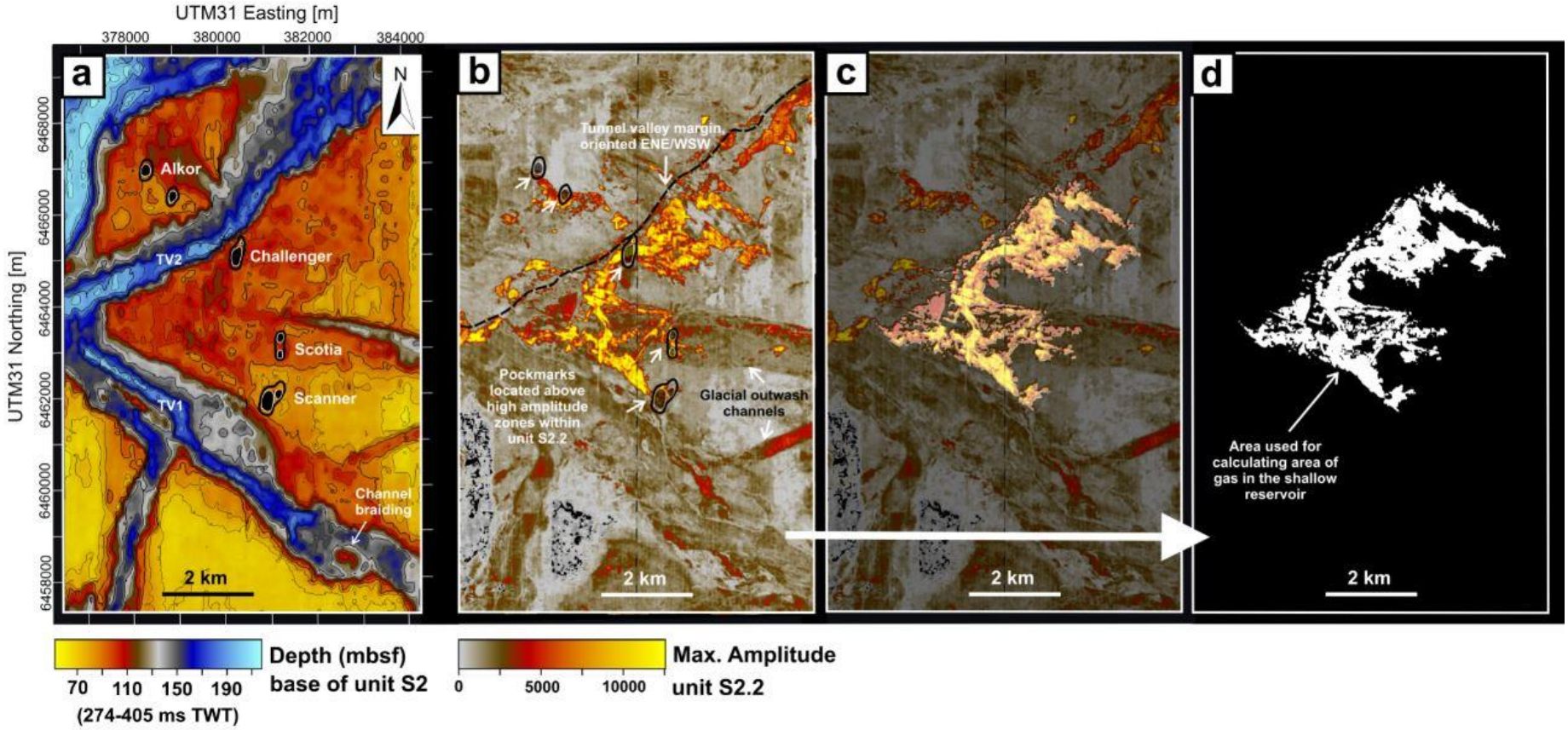

Supplementary Fig. S1. Glacial erosional features at base of the Ling Bank Fm. **(a)** Base of reflector S2 depth, **(b)** S2.2 maximum amplitude map from the 3D seismic reflection data. **(c-d)** The white zone highlights the area used for the gas volume calculations in the shallow reservoir. TV – Tunnel valley.

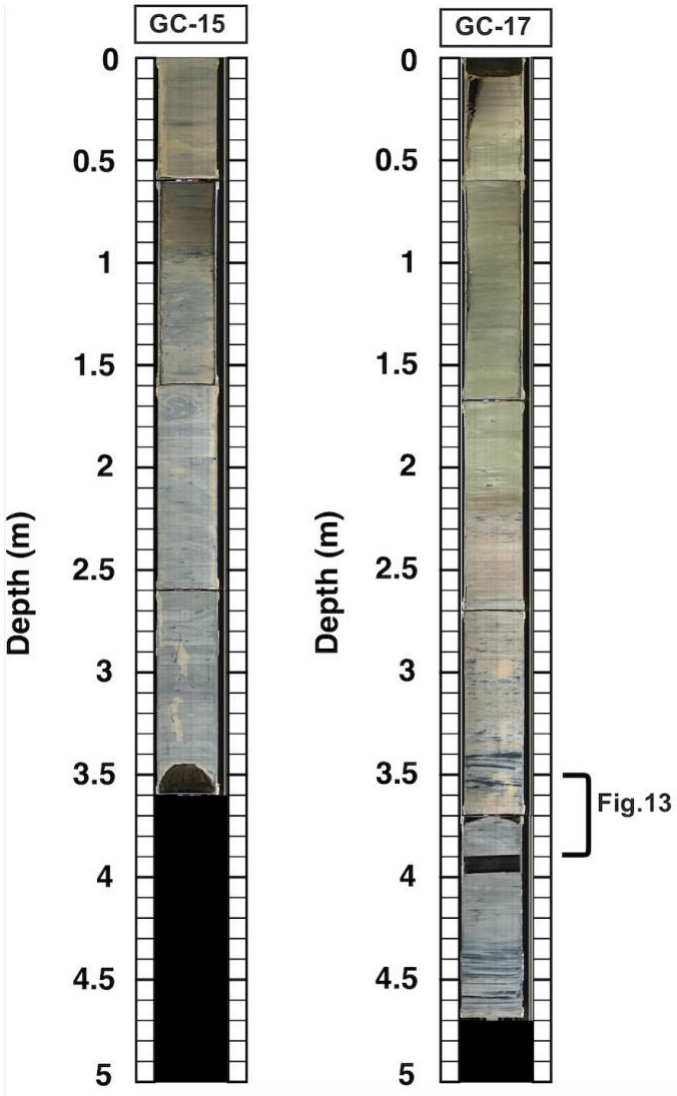

Supplementary Fig. S2. Photographs of gravity cores GC-15 and GC-17, extracted from below West (GC-15) and East (GC-17) Scanner pockmark (Figure 2b).

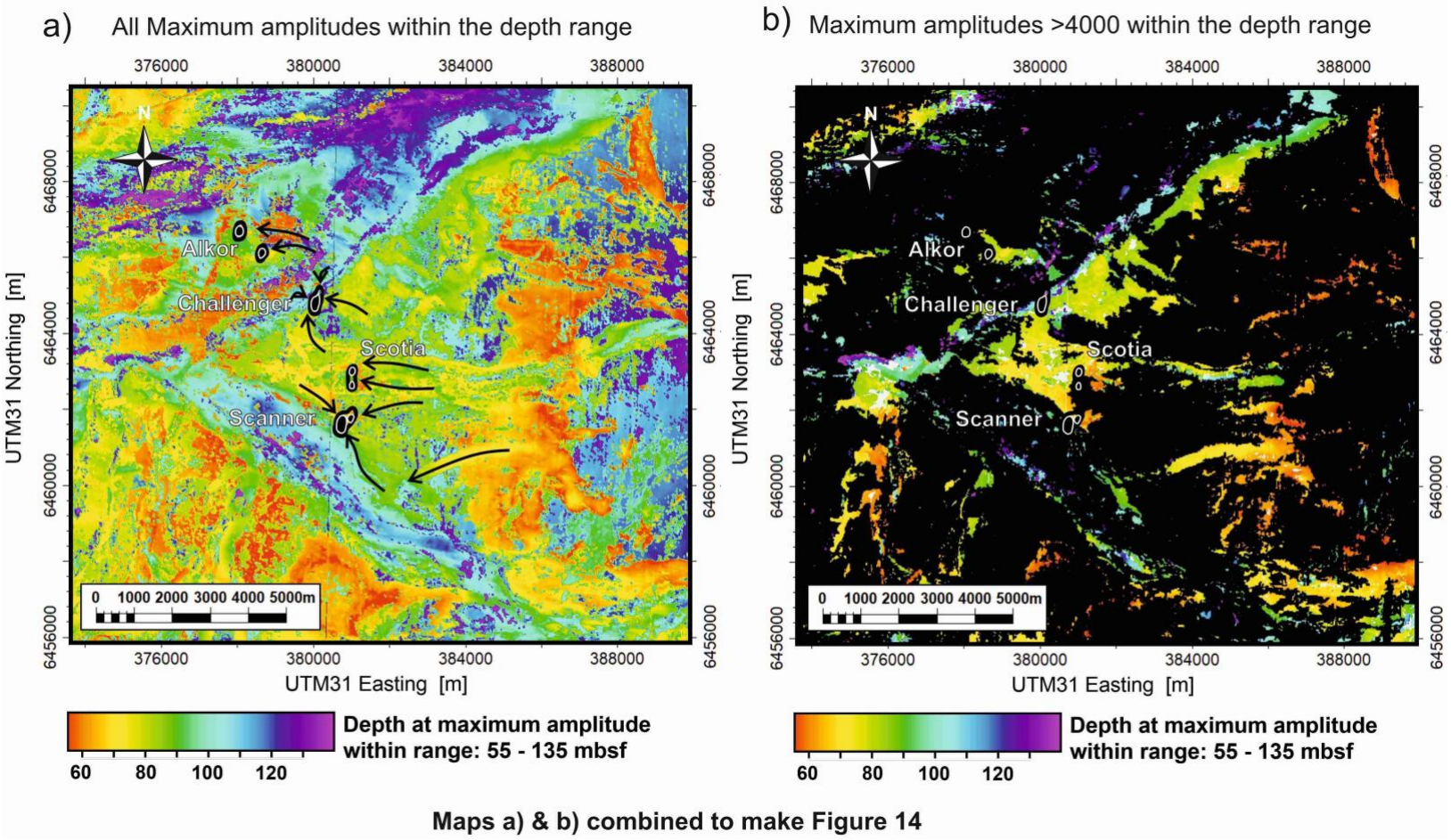

Supplementary Fig. S3. Distribution of gas-charged sediment across the Scanner pockmark complex from attribute analysis of 3D seismic reflection data. **(a)** The map shows the depth to the maximum amplitude in the depth range 55-135 metres below seafloor. Maximum amplitude is interpreted to correlate with the depth of gas charged sediment, as well as high impedance contrasts between clay-rich to sand-rich sediment. Black arrows indicate primary flow pathways towards the base of the large pockmarks. Locations of the large pockmarks are displayed using a black fill and dotted outlines. **(b)** brighter areas represent amplitude maxima corresponding to gas-saturated sediment (seismic amplitudes > 4000). Maps **a)** and **b)** are combined to make figure 14.

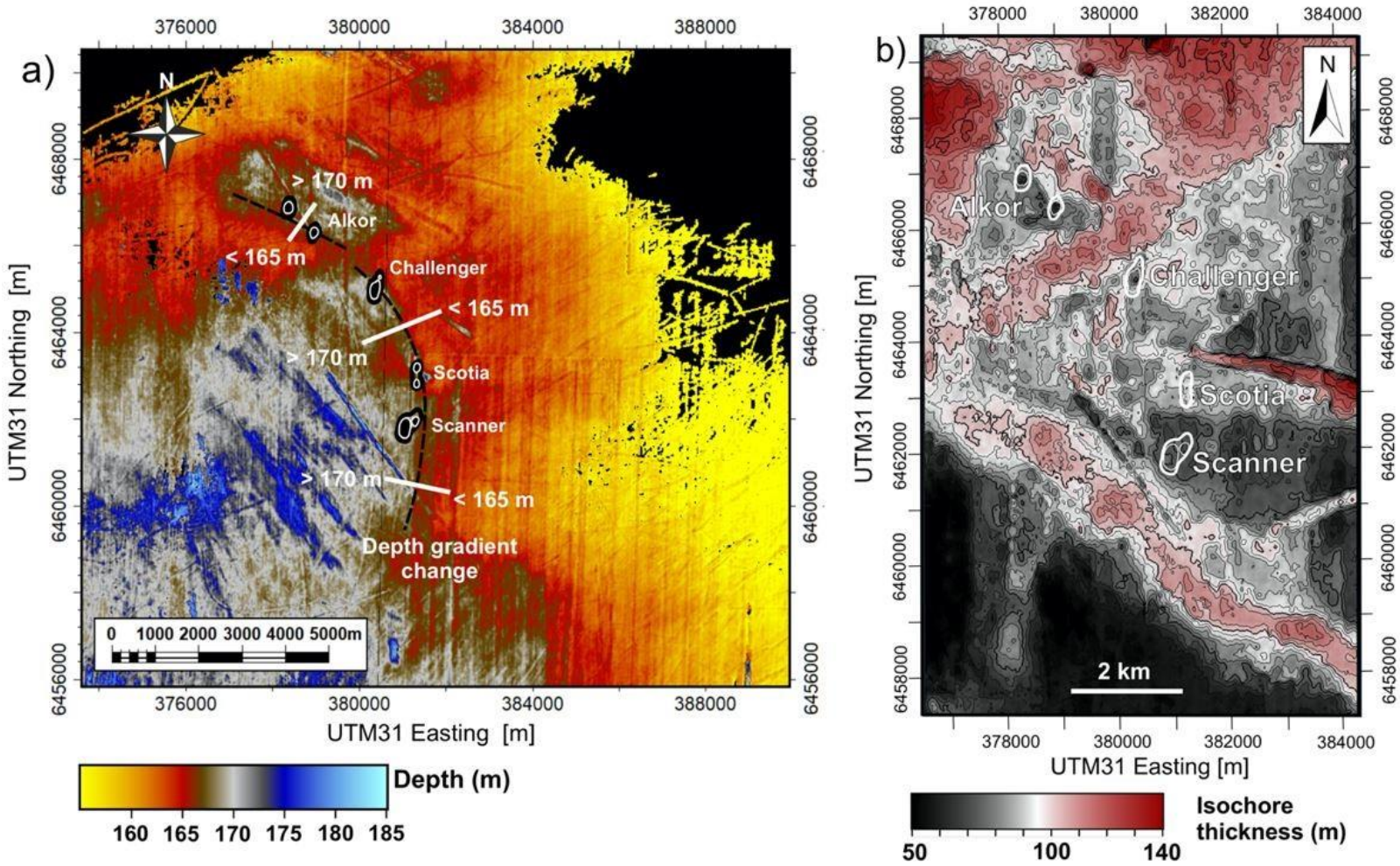

Supplementary Fig. S4. (a) Depth map of reflector base S5 (Witch Ground Fm) and **(b)** isochore thickness map from reflector base S5 to top S2.1 (basal unit of Ling Bank Fm). **a)** Near the large pockmarks, a 5 m depth increase is observed for reflector base S5. The comparatively sharp depth change (black dashed line) may cause localised focusing of fluid flow and subsequent overpressure generation in this stratigraphic interval. **b)** Areas of reduced isochore thickness correspond to the location of the large pockmarks. Therefore, it may be inferred that the pockmarks have formed in areas of reduced confining pressure/ overburden thickness.